to be submitted in Journal of Sedimentary Research

IGNEOUS ORIGIN OF CO_2 IN ANCIENT AND RECENT HOT-SPRING WATERS AND TRAVERTINES FROM THE NORTHERN ARGENTINEAN ANDES

ROGER O. GIBERT[1], CONXITA TABERNER[2]*, ALBERTO SÁEZ**[1], SANTIAGO GIRALT[2], RICARDO N. ALONSO[3], R. LAWRENCE EDWARDS[4] and JUAN J. PUEYO[5]

[1] Department of Stratigraphy, Paleontology and Marine Geosciences, University of Barcelona, Faculty of Geology, Martí Franqués s/n, E-08028 Barcelona, Spain

[2] Institute of Earth Sciences "Jaume Almera" (CSIC), Lluís Solé Sabarís s/n, E-08028 Barcelona, Spain

[3] Facultad de Ciencias Naturales, Universidad Nacional de Salta, Avda. Bolivia 5150, 4400 Salta, Argentina

[4] Department of Geology and Geophysics, University of Minnesota, USA

[5] Department of Geochemistry, Petrology and Geological Prospection, Faculty of Geology, University of Barcelona, Spain.

* Present address Shell International Exploration and Production B.V., 2288 GS Rijswijk (ZH), The Netherlands.

** Corresponding author: a.saez@ub.edu (Alberto Sáez)

Keywords: thermal travertines, stable isotopes, fluid inclusions, Pleistocene, Altiplano.

ABSTRACT: Thermal travertines are an archive of CO_2 sources and sinks in hydrothermal systems. Two major regional factors control travertine precipitation: water availability and CO_2 supply. Thus, travertines form a valuable archive of hydrodynamic variability and sources of main contributions to dissolved inorganic carbon (DIC). It is relevant to determine the main DIC sources of thermal waters (i.e., organic-matter degradation, recycled from older carbonates, emission of deep-seated magmatic CO_2), as they are key inputs to calculate the lithosphere - atmosphere CO_2 budget. The Antuco travertine from the Central Andes represents one of such archives, with a total of 500 ky record of accretionary periods (dated as 425-320, 260 and 155 ky BP) related to high hydrothermal activity of hot springs. It consist of two travertine units: (1) a lower massive unit displaying large calcite pseudomorphs after aragonite that precipitated in proximal ponds with

abundant water, and (2) an upper stratified unit showing more distal facies bearing siliciclastics and manganese and iron oxides. The replacement of aragonite by calcite in the lower unit was related to the decrease of water salinity in the thermal system through time. In the Antuco travertine, DIC $\delta^{13}C$ values of travertine parental waters of around -9‰ suggest that CO_2 was related to igneous processes and volcanic activity, and released along deep-seated faults. Relative water/rock ratios derived from $\delta^{18}O$ values and fluid-inclusion microthermometric data from travertine carbonates are consistent with an interpretation of greater water availability in the hydrothermal system during the Late Pleistocene than at present. The different petrographic features and isotopic signatures are interpreted to reflect increased water availability during more humid periods in the Altiplano, which triggered precipitation of travertine bodies. Travertine growth took place during interglacial-humid climate periods between Marine Isotope Stages (MIS) 3 and 9, which correspond to highstand events in large lakes of the Andean Altiplano. Results of this study illustrate that volcanic activity, furnishing rather constant CO_2 and heat fluxes, were the key controls of thermalism in the Altiplane region during the Quaternary, whilst climatic changes (humid vs. arid periods in the Late Pleistocene) controlled mineralogy, fàcies, and architecture of the travertines. The combined use of $\delta^{13}C$ and $^{87}Sr/^{86}Sr$ signatures in carbonate precipitates has been proven to be of major relevance to evaluate the CO_2 sources along fault zones in this study.

INTRODUCTION

Thermal travertines are an archive of CO_2 sources and sinks in hydrothermal systems (Moore et al. 2005). The most abundant travertine deposits are carbonate bodies precipitated in the proximity of thermal springs due to CO_2 outgassing, although silica and minor amounts of Fe-Mn oxides are also common. The main factors controlling travertine precipitation in hydrothermal systems are

CO_2 supply, meteoric water availability, heat source, and faults and fractures allowing deep-water (and solute) circulation (Frank et al. 2000).

In the Argentinean Altiplano of the Central Andes, hydrothermal circulation is driven by contemporary volcanism that provides rather constant heat sources and topographic gradients enabling deep-water circulation along major faults. Nevertheless, present-day hydrothermal activity in the region is limited to a few springs with low discharge, because water availability is constrained by present-day arid conditions (e.g., Klein et al. 1999; Godfrey et al. 2003). Nonetheless, travertine deposits are a common feature of the Altiplano in northwest Argentina, having formed mainly during Pleistocene humid periods in discharge areas of the Altiplano hydrothermal systems (Blasco et al. 1996). Travertine deposits in this region, such as those located in the proximity of Antofagasta de la Sierra (Alonso and Viramonte 1985) and San Antonio de Los Cobres (the present study), are closely linked in space and time to volcanism and tectonism. Although few studies provide data on the depositional architecture and geochemical aspects of travertine formation in the Altiplano (Rondeau 1990; Valero-Garcés et al. 2001), travertines formed in similar settings during the Pleistocene have been used to unravel climatic conditions (Rech et al. 2002) and to determine the timing of heat transfer in magmatic-thermal systems (Fournier 1989). Additionally, the use of geochemical signatures and petrographic features offers the potential to unravel the details of hydrothermal systems through the Pleistocene.

This study documents isotope and fluid-inclusion data from a Pleistocene hydrothermal travertine deposit in the Andean Altiplano, with the general aim of identifying the sources of CO_2 into the thermal system and the factors that controlled travertine deposition. This region in the Altiplano is characterized by arid conditions with low water availability and low soil CO_2 production, and as a result, the vegetation is too sparse to initiate any soil formation (Messerli et al. 1993) or to produce significant amounts of soil-derived CO_2, which by far is the most common carbon source for spring travertine formation (Pentecost 2005).

The results of this study illustrate how the petrographic features and the geochemical signatures of the Antuco travertine record changes in water availability in the Altiplano. The data reveal that the formation of the Antuco travertine deposits are the sink of deep-seated magmatic CO_2 sourced by hydrothermal waters flowing along a fault system related to a major lithospheric structure in a volcanically active area. As such, the travertine deposits of Antuco are an excellent archive of the influences of different CO_2 sources (endogenous vs. shallower sedimentary sources) and climate-derived hydrological changes. This study includes modern hot springs and their recent deposits, as well as older travertine deposits dating back to the Pleistocene. The workflow and environmental proxies used can be broadly useful in the interpretation of paleothermal systems.

GEOLOGICAL SETTING

The Antuco old travertine deposit (24º 10' S, 66º 40' W; 4,180 m above sea level) is located in the Argentinean Altiplano (Fig. 1). The travertine deposits are found cropping out over an area of about 0.5 km^2 along old quarry fronts. The Antuco travertine and other numerous travertine bodies in the region have been related to thermal waters flowing along the NW-SE Calama-Olacapato-Toro lineament (COT), a left-lateral transcurrent fault system about 700 km long (Allmendinger et al. 1983).

A NW-SE-trending volcanic belt developed along the COT fault in the Miocene (Coira et al. 1993; Matteini et al. 2002), and some of the presently -active volcanoes have been active since the Pliocene. Amongst them the Tuzgle is the only active volcano near the Antuco thermal spring (Fig. 1). The first record of the Tuzgle volcanic activity in the region corresponds to an ignimbrite that formed between 1.2 and 0.7 Ma. The last eruption of the Tuzgle volcano corresponds to a 0.1 Ma andesitic lava (Schwab and Lippolt 1974, Coira and Kay 1993). N-S-elongated Cenozoic

intermontane basins developed contemporaneous with the volcanic activity, on the Precambrian metamorphic-intrusive and Paleozoic-Mesozoic terrigenous basement rocks (Fig. 1). These basins were filled mostly by terrigenous sediments and interbedded lacustrine evaporites ("salars"). Carbonate rocks cropping out near the Antuco area are scarce and consist of marine limestones (Lower Ordovician, Las Vicuñas Fm; Upper Permian, Arizaro Fm; Upper Cretaceous-Paleocene, Yacoraite Fm; Blasco et al., 1996).

METHODS

Two field surveys (1998 and 2006) and sixty samples from the Antuco travertine deposits provided the basis for this study. In the samples, the mineral assemblage was determined using a Bruckner X-ray diffractometer (Cu Kα, 40 kV, 30 mA, and graphite monochromator). Fifty mirror-polished thin sections were petrographically examined to establish the paragenetic evolution of carbonate cements using optical, catodoluminescence (CL), and scanning electron (SE) microscopy. From the samples, five were selected for fluid-inclusion microthermometry, based on their representativeness of the different travertine facies and the presence of a sufficient number of fluid inclusions. The rock wafers were obtained using a low-speed wire-saw (Well) and, after a first low-pressure automatic polishing (Logitech) were hand-finished before being be analyzed for fluid-inclusion microthermometry. Fluid-inclusion associations (FIA, *sensu* Goldstein and Reynolds, 1994) could not be confidently identified due to the limited number of fluid inclusions in the travertines. Nevertheless, an attempt has been made to group the fluid inclusions from equivalent crystallographic positions (e.g., crystal growth zones, hairline fractures following cleavage) that potentially record similar growth conditions and parental fluids. Fluid inclusions from prismatic aragonite crystals and calcite rimming conduits were analyzed following standard procedures (Goldstein and Reynolds, 1994). The vapor:liquid ratios were calculated from the optical measurement of fluid-inclusion sizes and bubble diameters. A total of 76 determinations of

homogenization temperature and ice melting temperature were performed using a heating-freezing Linkam stage. Determination of the eutectic temperature was not feasible due to the small size and low salinity of the fluid inclusions. Aragonite fragments (0.15 g) were crushed under high vacuum (diffusion pump) and analyzed using an Extorr quadrupole to estimate the main evolved fluids.

Ten thick sections were used for $\delta^{13}C$ and $\delta^{18}O$ determinations. Fifty-seven micromilled samples (about 70 μg in weight) were drilled from selected precipitates and cements in the mirror-polished thick sections (150 μm -thick) with a Merchantek computer-monitored micromill. Use of a micromill provided pure samples of each carbonate cement phase, preventing isotopic contamination between phases. Once the mineralogy of each sample was determined and diagenetic alteration was excluded, $\delta^{13}C$ and $\delta^{18}O$ were measured in a Finnigan MAT 252 mass spectrometer equipped with a Kiel device. The results are expressed as per mil (‰), and the values are reported in relation to the Vienna Pee Dee Belemnite (V-PDB) international standard. The precision for both $\delta^{13}C$ and $\delta^{18}O$ for duplicate samples and standards is better than 0.1‰ (2σ). Four selected samples were also measured for $^{87}Sr/^{86}Sr$ in a Finnigan MAT 262 TIMS following a standard method (Pin and Bassin, 1992). The NBS-987 standard ($^{87}Sr/^{86}Sr = 0.710274$; $\sigma = 0.000016$) was used for accuracy and precision tests.

$\delta^{13}C_{CO2}$ values of the parental waters in isotopic equilibrium with the Antuco carbonates were calculated from the $\delta^{13}C$ of carbonates, the temperature of spring waters, and the homogenization temperature obtained from fluid inclusions. Water parameters in the present-day thermal spring (temperature, pH, and salinity) were measured during the field surveys. Water and air temperatures were measured with a thermometer. Waters were sampled separately for major and minor solutes and 1 vol% pure HNO_3 was added to water samples obtained for determination of minor solutes. Trace and minor solute contents were determined by ion chromatography and ICP-OS and ICP-MS following standard procedures. Additional samples were obtained for δD and $\delta^{18}O$ analyses and measured in a double-inlet mass spectrometer after equilibration with CO_2 (Epstein and Mayeda,

1953) and H_2 (Pt catalyst; Kirshenbaum, 1951; Horita et al., 1989) respectively. δD and $\delta^{18}O$ values are reported in ‰ *vs.* V-SMOW, and reproducibility of international standards and sample duplicates were, respectively, better than σ = 1.5 and 0.2‰.

Four samples from the Lower Travertine were dated with high-resolution U-series dating methods. U and Th were measured on an ICP-MS (Finnigan Element) following techniques developed at the Minnesota Isotope Lab (MIL) (Shen et al. 2002). Two more samples from the Upper Travertine were analyzed by alpha spectrometry following chemical separation and isotope electrodeposition procedures (Talvitie, 1972; Hallstadius, 1984; Bischoff et al. 1988). Age calculations were based on the computer program by Rosenbauer (1991).

RESULTS

The Present-Day Hot Springs: Water Chemistry and Precipitates

Thermal waters emanating from the Antuco springs were sampled and analyzed in 2006. Water had a temperature of 25ºC (air temperature of 12ºC when measured), a pH of 6.3, salinity around 1.8 wt%, and a flow rate of 5 L s^{-1}. The water type falls in the Cl-(SO_4-H_2CO_3)-Na group, with significant amounts of boron, lithium, iron, manganese, and arsenic. The chemical composition, in mg L^{-1}, was: 1075 DIC (as HCO_3^-), 9310 Cl^-, 2.5 NO_3^-, 1035 SO_4^{2-}, 5165 Na^+, 600 K^+, 530 Ca^{2+}, 150 Mg^{2+}, 150 Li^+, 490 BO_3^{3-}, 19 Si, 8.8 As, 5.3 Fe, 0.7 Mn, 10.5 Sr, 12 Rb, 0.044Ba. The isotopic compositions of this water were δD = -63.5 ‰ V-SMOW and $\delta^{18}O$ = -2.26 ‰ V-SMOW. A thin crust of iron-oxide-coated calcite is precipitated from the present-day waters near the spring and downstream.

The Antuco Travertine

The Antuco travertine deposits appear closely related to the Antuco hot springs (Fig. 1). These deposits consist of two main carbonate bodies (Lower Travertine and Upper Travertine) separated by a major unconformity and a piedmont breccia deposit (Fig. 2).

The Lower Travertine (LT) is the main carbonate body in the area and is located some 20 m away from the present-day hot springs. It is dome-shaped and about 8 m thick and 30 m wide. This lower travertine body is made up of centimeter- to decimeter-thick carbonate beds (Fig. 2). Travertine beds (Fig. 3A-C) are composed of calcite displaying pseudo-hexagonal twinned prismatic pseudomorphs after aragonite that reach up to 15 cm long and 4 cm wide. The shape and arrangement of the original aragonite crystals resemble those described in recent vent and proximal pond environments (Jones and Renaut 1996; Fouke et al. 2000). The originally aragonitic crystals have been extensively replaced by microsparite and sparry calcite. Porosity between the large aragonite crystals is partly filled by centimeter- to millimeter-size prismatic aragonite crystals, and millimiter-size aragonite needles and epitaxial overgrowths of calcite. Aragonite relics up to 5 mm across are still preserved with optical orientation following the original shape of the original crystals (Fig. 4).

Beds of the LT body are crossed by pipe-like conduits, rimmed by pink calcite crystals 1 to 15 cm- long (Fig. 4). These conduits are filled with micrometer-size iron and manganese oxide crystals. The conduit-rim calcite cements exhibit a columnar fabric (assemblage of roughly parallel, elongated calcite crystals, 0.1 mm to several centimeters in length) growing competitively inwards from the conduit walls. On the upper surface of the LT body, karstic cavities and cylindrical pits are partly filled with calcite cements with microcrystalline, dripstone, shrub, and columnar fabrics (with crystals up to 2 cm in length).

Piedmont alluvial deposits, 15 m- thick, overlie the Antuco LT (Fig. 2). They are composed of poorly cemented depositional breccias with large and angular volcanic clasts (up to 1 m- long) that

cover the Lower Travertine body and the karst surface. Fragments of the LT have been identified within the breccias, illustrating the timing of their formation.

The Upper Travertine (UT) body is located about 100 m downstream from the present-day hot springs and overlaies the piedmont alluvial deposits. It consists of interbedded convex-concave sandstone layers and grey bedded travertine (Fig. 2) with variable amounts of volcanic clasts and carbonate fragments. Centimeter- to decimeter-thick layers of manganese and iron oxides are common near the basal part of the UT body. The main fabrics of this UT body consist of microsparite and shrub calcite crystals (*sensu* Chafetz and Guidry, 1999) up to 4 cm- long with relics of cyanobacterial filaments. Fabrics and sedimentary structures of this travertine body correspond to proximal and distal slope facies (*sensu* Fouke et al. 2000).

Age of Travertines

The terrigenous content of the dated samples is negligible since the $^{230}Th/^{232}Th$ ratio values are low (Table 1) and can be considered as not contaminated. Uranium-series disequilibrium dating indicates that the Antuco LT beds precipitated between 427 ± 60 and 324 ± 27 ky BP (aragonite crystal samples) and that conduit-rim calcite cements formed at 259 ± 30 ky BP. A sample located 15 cm below the top of the UT deposit yielded an age of 156 ± 11 ky BP (Table 2, Fig. 2).

Isotopic Data of Waters and Precipitates

The $\delta^{13}C_{V\text{-}PDB}$ values of the LT mound carbonates range between -4.1 and -5‰, and the $\delta^{18}O_{V\text{-}PDB}$ values from -21.2 to -22.4‰. The $\delta^{13}C_{V\text{-}PDB}$ values of the conduit-rim calcite cements vary between -5.5 and -6‰, and the $\delta^{18}O_{V\text{-}PDB}$ values between -21.7‰ to -22.6‰. Karst-related carbonates record $\delta^{13}C_{V\text{-}PDB}$ values between -2.1 and -4.3‰ and $\delta^{18}O_{V\text{-}PDB}$ between -14.2 and -19.1‰ (see Data Archive, Figs. 3C and 5A).

The carbonate travertine of the UT body includes $\delta^{13}C$ and $\delta^{18}O$ values that are distinct from the isotopic compositions of those in the LT body. The $\delta^{13}C_{V\text{-}PDB}$ values range between +1.6 and +5‰, whereas the $\delta^{18}O_{V\text{-}PDB}$ between –4.6 to -11.7‰ (see Data Archive, Figs. 3C and 5A).

The isotopic composition of present-day thermal waters ($\delta^{18}O_{V\text{-}SMOW}$ = -2.3‰) is enriched in ^{18}O with regard to the regional meteoric water (snow sample: $\delta^{18}O$ = -10.3‰; Godfrey et al. 2003), whilst the δD ($\delta D_{V\text{-}SMOW}$ = -63.5‰) is similar (snow sample: $\delta D_{V\text{-}SMOW}$ = -60.9‰). The $\delta^{13}C_{V\text{-}PDB}$ values of the thin iron-oxide-coated calcite crusts that precipitate from thermal water near the spring oscillate between +2.9 and +3.1‰ and their $\delta^{18}O_{V\text{-}PDB}$ values between -1.3 and -1.1‰ (see Data Archive, Fig. 5A and B). These $\delta^{18}O$ values suggest isotopic equilibrium between present-day thermal waters and recent calcite precipitates when applying the Friedman and O'Neil (1977) equilibrium equation. $^{87}Sr/^{86}Sr$ values in two samples of aragonite from the LT carbonates are respectively 0.720274 and 0.720595. Two samples of calcite from the UT body display values of 0.718561 and 0.718768.

Temperature and Salinity of the Lower Travertine Parental Waters

Fluid inclusions occur in the primary prismatic aragonite crystals and in calcite crystals rimming the pipe-like conduits in the LT, but they are absent in the UT precipitates and in the karst-related cements. The following three main groups of fluid inclusions are evident in the LT:

Group 1. This group corresponds to fluid inclusions in preserved aragonite crystals (Figs. 4 and 6). These primary fluid inclusions, elongated 12 to 20 μm- long and 2 - 4 μm- wide, lie parallel to the aragonite crystallographic *c* axis (Fig. 7). This group has two-phase inclusions with a vapor-liquid (V-L) ratio of about 9 vol % on average. Some populations of fluid inclusions show inconsistent ratios (vapor bubbles from 7 to 60 vol %) and, in some crystal zones, include liquid-only inclusions. The originally elongated primary fluid inclusions (with consistent vapor:liquid ratio) appear to pass into a succession of aligned smaller fluid inclusions with variable vapor:liquid

ratios, suggesting that stretching processes have partially affected this population. These inclusions with stretching patterns were rejected for microthermometric purposes following the recommendations of Goldstein and Reynolds (1994) and Bodnar (2003). The 15 measured primary liquid-vapor inclusions display homogenization temperatures ranging from 76 to 98ºC and ice melting temperatures between -1.5 and -2.7ºC (3.1 to 4.5 wt % NaCl equivalent; Bodnar, 1993). The mean value of the homogenization temperature is 87.5ºC, and the mean salinity for the parental waters is 3.4 wt % NaCl equivalent (Table 3, Fig. 6). The main fluid released by crushing under vacuum of two aragonite crystalline samples, including both FI groups 1 and 2, was water steam (around 90 vol %) with minor amounts of N_2 and O_2 (around 8% of N_2 and O_2) and CO_2 (2%). The low value of atmospheric gases eliminates boiling as a process responsible for the inconsistent vapor:liquid ratios. No CO_2 bubbles are observed in the fluid inclusions, which is consistent with the very low CO_2 content measured in the extracted fluids

Group 2. These fluid inclusions are also present in the aragonite crystals (Fig. 8). They intersect the Group 1 fluid-inclusion assemblages obliquely with respect to the aragonite *c* axis, following cleavage planes. These inclusions are small (diameter ranging from 5 to 20 μm; average about 8 μm) with vapor:liquid ratios between 6 and 12 vol % (Fig. 8). The 33 fluid inclusions measured from this population display homogenization temperatures from 95 to 110ºC and ice melting temperatures between -0.6 and -1.5ºC (1.1 to 2.6 wt % NaCl equivalent; Bodnar, 1993). The mean value of the homogenization temperature is 106.5ºC, and the mean salinity of the parental waters is 1.4 wt % NaCl equivalent (Table 3, Fig. 6).

Group 3. These fluid inclusions are located in the conduit-rim calcite cements (Fig. 9). They consist of two-phase inclusions with an average diameter of 9 μm (range from 5 to 20 μm). The inclusions are arranged along the growth zones of the columnar calcite crystals (Fig. 4) and commonly exhibit negative crystal shapes (Fig. 9). The 28 fluid inclusions measured from this population display homogenization temperature values from 103ºC to 132ºC and ice melting

temperature values between -0.3ºC and -0.6ºC (0.5 to 1.1 wt % NaCl equivalent; Bodnar, 1993). The mean value of the homogenization temperature is 115.2ºC, and the mean salinity value of the parental waters is 0.9 wt % NaCl equivalent (Table 3, Fig. 6).

DISCUSSION

Evolution of Thermal Water

Travertines are shaped by hydrothermal processes, and these commonly vary with time. The geochemical and petrographic evidence in this area clearly illustrates the nature and timing of this variability. In this study, $\delta^{18}O_{V\text{-}SMOW}$ values of parental waters were calculated from travertine $\delta^{18}O$ values and homogenization-temperature data of primary inclusions using the well-established fractionation equations between water and aragonite (Zheng, 1999; Bahm et al. 2000) and between water and calcite (O'Neil et al. 1969; Friedman and O'Neil 1977). The results illustrate that LT aragonite crystals precipitated from low-salinity waters with $\delta^{18}O_{V\text{-}SMOW}$ values similar to those of present-day regional meteoric water (Fig. 5B) at temperatures of about 87ºC (boiling point of water at Antuco). Although the parental waters were hot and circulated through the thermal system, they maintained the original meteoric isotopic signature and their $\delta^{18}O$ values did not show major changes due to water-rock interaction. The measured homogenization temperatures in the LT suggest that aragonite precipitated from boiling water under atmospheric pressure.

In contrast, calcite crystals that replace aragonite and karst-related precipitates have higher $\delta^{13}C$ and $\delta^{18}O$ values than the primary LT carbonates, and their isotopic values follow a positive trend (Fig. 5A). This trend is explained by the cooling, as suggested by microthermometrical data, and outgassing of thermal waters that circulated through the travertine body, triggering precipitation of replacive calcite and karst-related cements. These karst-related cements record the highest $\delta^{13}C$ and

$\delta^{18}O$ values in the LT carbonates, suggesting that the karst system formed from cooled and outgassed thermal waters.

The homogenization temperature (115ºC) of the conduit-rim calcite cement (group 3) fluid inclusions and the $\delta^{18}O$ values of calcite (-22.2‰) suggest that it precipitated from waters with $\delta^{18}O_{V\text{-}SMOW}$ values (about +2.5‰) higher than those precipitating the main travertine body (Fig. 5B), which provides evidence of water-rock interaction along thermal-water pathways. The higher homogenization temperatures suggest that these rimming calcite crystals formed under hydrostatic pressure equivalent to about 15 m of water column.

The homogenization temperatures recorded in the Group 2 fluid inclusions (106ºC) are considerably higher than those from the primary fluid inclusions of Group 1 (87ºC) and similar to fluid inclusions of Group 3. This observation suggests that the replacement of aragonite occurred as a result of the circulation of thermal fluids through the travertine body under hydrostatic pressure (Fig. 4). Fluid-inclusion data (from Group 1 to Groups 2 and 3) record a temporal trend towards hotter and less saline thermal waters (Fig. 6C). Less saline waters, similar to the group 3 fluid inclusions, were in disequilibrium with aragonite, causing their replacement by secondary calcite in a later stage of the evolution of the LT body. Evidence of this alteration process has been found in the aragonite relics (Fig. 4): besides the primary fluid inclusions (Group 1 of FI) that correspond to original aragonite-crystal parental waters, Group 2 of FI, located along cleavage plains in the aragonite relics, records the circulation of lower-salinity and higher-temperature late fluids.

$\delta^{18}O$ values of LT parental waters and of present-day thermal waters were taken as the end-members of the water evolution trend during the last 500 ka (Fig. 5B). The $\delta^{18}O_{V\text{-}SMOW}$ of parental waters precipitating the gray travertine (UT body) was calculated from the trend of parental water evolution in accordance with their age. In these, isotopic values range between -6.2 to -4.2 ‰ (Fig. 5B). The temperatures of precipitation (29 to 38ºC) of the UT body were calculated from the mean $\delta^{18}O_{V\text{-}PDB}$ of UT carbonate values and from parental-water $\delta^{18}O_{V\text{-}SMOW}$ values.

Water temperature in thermal systems depends on of the dynamics of the convection cells. The observation of present-day temperature of the spring waters (around 25ºC) is interesting in this regard. Low temperatures (or temperature changes) in thermal springs have been interpreted as due to mixing of thermal waters with shallower aquifers (López-Chicano et al. 2001; Dilsiz et al. 2004). Nonetheless, the Antuco spring waters do not show clear evidence of mixing, for the following three reasons: (1) the thermal water is very rich in, B, Li, and As and shows Fe (and Mn) mineral precipitates, (2) water salinity values are also in the range of paleosalinities calculated from microthermometric measurements in the lower travertine (stage of deep and highly efficient convection cell), and (3) $\delta^{18}O$ values of thermal waters are very high with regard to meteoric water. Instead, the low temperature is interpreted to be related to the very high rock/water ratio. In this scenario, the heat transport is limited due to the scarcity of water, and thus the temperature of waters reaching the surface is low.

Values of salinity around 4 wt % NaCl, similar to those measured in the Group 1 fluid inclusions (in aragonite relics), have been reported as common in convective systems around magmatic intrusions (Cathles, 1977). In the case of Tuzgle volcano, the presence of free saline fluids at 8 km depth has been documented using magnetotelluric and gravity measurements (Sainato and Pomposiello, 1997).

Carbon Source

Soil-derived CO_2 is by far the most common source of carbon to spring travertine waters (Pentecost, 2005). The $\delta^{13}C$ value of pedogenic carbonates is controlled by the predominant vegetation type in the region, but carbon can be fractionated differently as a function of the photosynthetic pathway of plants growing in the soil. $\delta^{13}C$ values range between -30 and -16‰ for C3 plant soils and between -18 and -10‰ for C4 plant soils (Vogel, 1993), although C4 plants are scarce in high-elevation regions (Quade et al. 1989; Rech et al. 2002). Thus, values of $\delta^{13}C$ around -6‰ for LT carbonates (around -9‰ for CO_2, as derived from the equations in Bottinga, 1969;

Ohmoto and Rye, 1979; and Romanek et al. 1992) in the Altiplano area are consistent with carbon dioxide being supplied mostly by igneous sources (Craig, 1963; White et al. 1990; Hoefs, 1997; Pentecost, 2005).

The $\delta^{13}C$ difference (about 8‰) between both travertine bodies (Fig. 5A) might suggest a change in the carbon source. The increase in $\delta^{13}C$ (and $\delta^{18}O$) in the UT could be interpreted as resulting from recycling of marine limestone units (Blasco et al. 1996) present at depth in the area. Isotopic mixing of $\delta^{13}C$ from these older marine carbonates (with assumed values approximately between -2 and +5 ‰; Garrels and Lerman, 1981; Carpenter and Lohmann, 1999; Prokoph et al. 2008; Marquillas et al. 2007) would be irrelevant with respect to the igneous signature (accepted around -7 to -6 ‰; Hulston and McCabe, 1962; Craig, 1963; Ferrara et al. 1963; White et al. 1990) that clearly dominates along the LT deposition (Fig. 10). However, the contribution of CO_2 of carbonate origin could have increased during UT deposition that displays $\delta^{13}C$ in the range of the marine carbonates, due to the lower water/rock ratios evident during its formation (*sensu* Taylor, 1987). $^{87}Sr/^{86}Sr$ values in the Antuco travertines show a strong radiogenic signature (Fig. 10) consistent with a source from leaching of old silicate basement rocks (Fig. 1; Precambrian and Paleozoic). The LT of Antuco records high radiogenic signatures (around 0.7204), similar to those reported in the Menderes Massif geothermal system (SW Turkey) for thermal waters that interact with metamorphic rocks (Vengosh et al. 2002, 2003). The same authors found much lower values (around 0.7078) for the Pamukkale (Turkey) thermal travertines, evidencing the recycling of marine Paleozoic carbonates present in the basement. The $^{87}Sr/^{86}Sr$ values in the Antuco UT, although strongly radiogenic and far from the marine values, as would correspond to a Pamukkale-like recycling, are slightly lower than the LT ones (Fig. 10). Nevertheless, these values do not follow a $\delta^{13}C$ - $^{87}Sr/^{86}Sr$ trend that would be expected in the presence of fluid mixing between the LT and marine carbonates. Thus, the observed $\delta^{13}C$ trend cannot be explained as a result of contributions from recycling of older carbonates. Other sources of carbon, like the leakage from hydrocarbon

reservoirs releasing CO_2 (e.g., Davies and Smith, 2006), have been discarded based on the following:

(1) A hydrocarbon-related source commonly causes very low values (lower that -10‰; e.g., Zhang et al. 2008) or a large variability of values, when mixed with other contributions. The $\delta^{13}C$ of calcite and aragonite precipitates are remarkably constant for the LT unit. More variability would be expected in case of mixtures of hydrocarbon-related and carbonate-recycled CO_2.

(2) There is no geological evidence of hydrocarbons in the studied area. The Yacoraite Formation contains hydrocarbons at locations hundreds of kilometers eastwards, out from the Altiplano. The equivalents in the Antuco area consist of shallow-water calcarenites with no recorded presence of hydrocarbons (Alonso et al. 1984; Marquillas et al. 2007).

The $\delta^{13}C$ values of the UT samples fit better with a fractionation trend of outgassing and cooling (Zheng, 1990). Isotopic fractionation between CO_2 and aragonite or calcite is well known in a wide range of temperatures (see equations in Bottinga 1969, Ohmoto and Rye 1979, and Romanek et al. 1992). The calculated $\delta^{13}C$ values of the parental CO_2 do not vary considerably between the two travertine bodies, which suggests that the $\delta^{13}C$ difference could result mainly from fractionation at different temperatures. Calculated parental $\delta^{13}C_{CO2}$ values during precipitation of the Antuco LT are around -9‰, similar to present-day carbonates, whereas the UT carbonates, which precipitated distally from the spring at temperatures between 28 and 39ºC (calculated from the water evolution trend; see above), record parental $\delta^{13}C_{CO2}$ values that range between -6.8 and -5.9‰. These slightly higher $\delta^{13}C$ values for the UT can be attributed mostly to the outgassing effect that favors escape of light CO_2 from spring waters (White et al. 1990; Valero et al. 1999; Valero et al. 2001; Cartwright et al. 2002).

At present, the Tuzgle stratovolcano is the only active volcano in the region (De Silva and Francis 1991), and its magmatic chamber may constitute the heat and CO_2 source of the Antuco hydrothermal system. Nevertheless, there are also other (Pliocene-Pleistocene) volcanic centers in

the area such as Tocomar (0.55 Ma), Negro de Chorrillos (0.45 Ma), and San Jerónimo (0.78 Ma) that have erupted along the COT during the Pleistocene (Coira et al. 1993; Petrinovic et al. 2006). These could also be magmatic CO_2 sources in the region. Nonetheless, it seems that heat and CO_2 sources can be considered practically ”constant” in the area over the last million years, in that (1) the available information on thermal gradients and fluxes around magmatic intrusions suggests cooling times in the order of 10^6 years (Ingebritsen et al. 2001, Deckart et al. 2005) and (2) the Tuzgle stratovolcano has been active during the last million years.

Paleoclimate and Water Availability

The primary source of precipitation in the Altiplano region in the Central Andes is related mainly to the arrival of Atlantic moisture via the Amazon Basin (Garreaud et al. 2003). The high lake levels recorded in the large lakes of the Altiplano (Titicaca, Salar de Atacama, and Uyuni Basin lakes) during the interglacial-warm stages (from MIS 3 to MIS 9) suggest humid climate conditions. Their low lake level stages correspond to glacial stages (from MIS 4 to MIS 8) (Bobst et al. 2001; Fritz et al. 2004; Fritz et al. 2007; Placzek et al. 2006). Nevertheless, humid conditions prevailed during the Last Glacial Maximum in the Altiplano (Baker et al. 2001; Fritz et al. 2004; Sáez et al. 2007) (Fig. 11). This correspondence between maximum summer insolation on the Altiplano Plateau and increased moisture availability during the Late Pleistocene suggests an orbital control of the South American summer monsoon (Strecker et al. 2007).

The Antuco record spans from MIS 6 to MIS 9, but it is not continuous, because of stratigraphic hiatuses. The Antuco travertines were formed during three main growth periods, as constrained by the hydrothermal activity (Fig. 11), which correspond roughly to the interglacial-humid and glacial-dry climate pattern of the Altiplano between ca. 350 and 57 kyr BP. The $^{238}U/^{230}Th$ age dates illustrate that the first growth event, the lower travertine body (LT), was formed during the humid interglacial of MIS 9. The second event, evident in the stockwork of pipe-like conduits, which

clearly crosscuts the LT beds, was formed around 60,000 years later than the LT body, during the dry MIS 8 and/or the humid MIS 7. The third travertine growth event corresponds to the Upper Travertine (UT) body, which was deposited during the dry MIS 6.

The similar $\delta^{18}O_{V\text{-}SMOW}$ values of LT parental waters and recent regional meteoric waters (Godfrey et al. 2003) (Fig. 5B) suggest that the LT travertine precipitated during periods of high availability of meteoric water in the thermal system. High water/rock ratios helped to maintain the original $\delta^{18}O$ signature of meteoric waters. Homogenization temperatures, close to the water boiling point at the Altiplano altitude, and textural features such as the limpid aragonite crystals devoid of clastic impurities, indicate that the LT aragonite precipitated close to the spring, probably in pools.

Isotopic and fluid-inclusion data obtained from the conduit-rim calcite cement, with homogenization temperatures higher than the boiling point at the Altiplano surface, suggest that these carbonates formed in vents and precipitated from evolved thermal waters in conditions of lower water/rock ratio and higher $\delta^{18}O_{V\text{-}SMOW}$ of parental waters than the previously precipitated travertines (Fig. 5B). These conduits were formed around 260 ky BP (MIS 7-8) when the hydrological conditions were intermediate compared to the other periods of travertine growth (Fig. 11). From 260 ka to the present, the general increase of $\delta^{18}O$ in carbonates and their lower formation temperatures (either interpreted or measured) reflect a decrease in the water/rock ratio, suggesting an increase in aridity towards the present-day conditions (Fig. 5B).

The high $\delta^{18}O_{V\text{-}SMOW}$ values of the UT parental waters and of the present-day calcites (Fig. 5B) suggest a decrease in the water/rock ratio. The UT was formed during more arid conditions and lower water availability, and it coincides with a glacial stage (ca. 155 ky BP, MIS 6; Fig. 11). The presence of cyanobacterial filaments and clastic materials in these carbonates also suggest that they precipitated in downstream pools. These distal pools (or distal slope facies) commonly develop a rich variety of living organisms arranged along the thermal and chemical gradient (Renaut and

Jones 2000; Fouke et al. 2000). Also, distal pools commonly contain clastic remains, either from outside the thermal system or produced by internal reworking.

CONCLUSIONS

Neogene volcanic activity and variations in the moisture content in the Central Andes influenced the formation of large travertine deposits in the Altiplano during the Late Pleistocene. Carbonates of the Antuco thermal travertine bodies precipitated during the last 500 ka, during which time changes in water availability are reflected in different petrographic features and isotopic compositions.

In this area, three main periods of travertine growth are related to different phases of water availability that roughly agree with interglacial-humid periods in the Altiplano: (1) growth of the Lower Travertine body, about 425 and 320 ky BP, when water availability was high, (2) formation of the stockwork of vents crossing the LT about 260 ky BP, when water availability was intermediate, and (3) deposition of piedmont and the Upper Travertine body about 155 ky BP, when water availability was low.

Isotopic trends of carbonate minerals and parental water reflect changes in the water supply that fed the Antuco thermal system during the last 500 ka. Late Pleistocene humid conditions assured a high water supply and a high water/rock ratio, favoring precipitation of travertines in pools from waters with low $\delta^{18}O_{V\text{-}SMOW}$ values (meteoric waters not modified through rock-water interaction). From 260 ky BP to the present, water/rock ratios decreased as a consequence of increasing aridity, resulting in precipitation of carbonates enriched in ^{18}O.

Calculated parental $\delta^{13}C_{CO2}$ values (around -9‰ V-PDB) of the Antuco travertines indicate a stable and dominantly igneous CO_2 source in thermal waters during the last 500 ka. Igneous CO_2 dissolved under pressure in thermally heated groundwater was fed through deep-seated faults. The outgassing of these CO_2-rich rising waters at the surface drove travertine precipitation.

All geochemical and regional evidence is consistent with a model of a dominantly igneous origin of CO_2 in the Antuco springs. This magmatic signature is clearly recorded in the $\delta^{13}C$ of carbonate precipitates near vent locations, with limited fractionation due to outgassing (LT unit and present-day carbonates). The trend towards higher $\delta^{13}C$ values in the younger UT unit, formed by distal slope facies, indicates modification of the primary carbon isotopic signature (endogenous here) by surface cooling and outgassing of CO_2. The Antuco travertines can be considered as an example in which, in spite of the presence of old carbonate formations in the area, their was a clearly dominant deep-seated magmatic source of CO_2. The combined use of $\delta^{13}C$ and $^{87}Sr/^{86}Sr$ signatures has been of major relevance to track the source of CO_2 leakage and sink along fault zones in this study.

ACKNOWLEDGMENTS

This work was supported by the Spanish Ministry of Education and Science (MEC) through the projects AYIN93-000547; ANDESTER (BTE2001-3225); BTE2001-5257-E, LAVOLTER (CGL2004-00683), and GEOBILA (CGL2007-60932). MEC also provided the funding to carry out the research stages of R.O. Gibert at the University of Minnesota and Universidad Nacional de Salta. We are grateful to the *Scientific-Technical Services* of the University of Barcelona for the C and O stable-isotope analyses, to the *Ibercron Laboratory* of the Basque Country University at Bilbao for the $^{87}Sr/^{86}Sr$ data, and to the technicians of the Institute of Earth Sciences "*Jaume Almera*" (CSIC) for performing the and alpha-spectrometry determinations. We are also indebted to the reviewers and editors Don Hall, John Luczaj, Kathy Benison, Eugene Rankey, and John B. Southard. Their careful review and comments have strongly improved the original manuscript.

REFERENCES

Allmendinger, R.W., Ramos, V.A., Jordan, T.E., Palma, M., and Isacks, B.L., 1983, Paleogeography and Andean structural geometry, northwest Argentina: Tectonics, v. 2, p. 1-16.

Alonso, R.N., and Viramonte, J., 1985, Geyseres boratíferos de la Puna Argentina: IV Congreso Geológico Chileno, Actas II, p. 23-44, Antofagasta.

Alonso, R.N., Viramonte, J.G. ,and Gutierrez, R., 1984, Puna Austral. Bases para el subprovincialismo geológico de la Puna Argentina: IX Congreso Geológico Argentino, Bariloche, Actas I, p. 43-63.

Bahm, F., Joachimski, M.M., Dullo, W.C., Eisenhauer, A., Lehnert, H., Reitner, J., and Worheide, G., 2000, Oxygen isotope fractionation in marine aragonite of coralline sponges: Geochimica et Cosmochimica Acta, v. 64, p. 1695-1703.

Baker, P.A., Rigsby, C.A., Seltzer, G.O., Fritz, S.C., Lowenstein, T.K., Bacher, N.P., and Veliz, C., 2001, Tropical climate changes at millennial and orbital timescales in the Bolivian Altiplano: Nature, v. 409, p. 698-701.

Bischoff, J.L., Julià, R., and Mora, R., 1988, Uranium-series dating of the Mousterian occupation at Abric Romaní, Spain: Nature, v. 332, p. 68-70.

Blasco, G., Zappettini, E., and Hongn, F., 1996, Hoja Geológica 2566-I, San Antonio de los Cobres (Jujuy, Salta), Boletín n° 217, mapa 1:250.000: Dirección Nacional del Servicio Geológico, Buenos Aires.

Bobst, A.L., Lowesnstein, T.K., Jordan, T.E., Godfrey, L.V., Ku, T.-L., and Luo, S., 2001, A 106 ka paleoclimate record from drill core of the Salar the Atacama, northern Chile: Palaeogeography, Palaeoclimatology, Palaeoecology, v. 173, p. 21-42.

Bodnar, R.J., 1993, Revised equation and table for determining the freezing point depression of H_2O-NaCl solutions: Geochimica et Cosmochimica Acta, v. 57, p. 683-684.

Bodnar, R.J., 2003, Introduction to Fluid Inclusions: Mineralogical Association of Canada, Short Course 32, p. 1-9.

Bottinga, Y., 1969, Calculated fractionation factors for carbon and hydrogen isotope exchange in the system calcite-carbon dioxide-graphite-methane-hydrogen-water vapour: Geochimica et Cosmochimica Acta, v. 33, p. 49-64.

Carpenter, S.J., and Lohmann, K.C., 1999, Reply to the comment by S.T. Petsch on Carbon isotope ratios of Phanerozoic marine cements: re-evaluating global carbon and sulfur systems: Geochimica et Cosmochimica Acta, v. 63, p. 761-766.

Cartwright, I., Weaver, T., Tweed, S., Ahearne, D., Cooper, M., Czapnik, K., and Tranter J., 2002, Stable isotope geochemistry of cold CO_2-bearing mineral spring waters, Daylesford, Victoria, Australia: sources of gas and water and links with waning volcanism: Chemical Geology, v. 18, p. 71-91.

Cathels, L.M., 1977, An analysis of the cooling of intrusives by ground-water convection which includes boiling: Economic Geology, v. 72, p. 804-826.

Chafetz, H.S., and Guidry, S.A., 1999, Bacterial shrubs, crystal shrubs, and ray-crystal shrubs: bacterial vs. abiotic precipitation. Sedimentary Geology, v. 126, p. 57-74.

Coira, B., and Kay, S.M., 1993, Implications of Quaternary volcanism at Cerro Tuzgle for crustal and mantle evolution of the Puna Plateau, Central Andes, Argentina: Contributions to Mineralogy and Petrology, v. 113, p. 40-58.

Coira, B., Kay, S.M., and Viramonte, J., 1993, Upper Cenozoic magmatic evolution of the Argentine Puna – A model for changing subduction geometry: International Geology Review, v. 35, p. 677–720.

Craig, H., 1963, The isotopic geochemistry of water and carbon in geothermal areas, *in* Tongiorgi, E. ed., Nuclear Geology on Geothermal Areas: Pisa, Consiglio Nazionale delle Ricerche, Laboratorio di Geologia Nucleare, p. 17-53.

Davies, G.H., and Smith, L.B. Jr., 2006, Structurally controlled hydrothermal dolomite reservoir facies: An overview: American Association of Petroleum Geologists, Bulletin, v. 90, p.1641–1690.

Deckart, K., Clark, A.H., Celso, A.A., Vargas, R., Bertens, A.N., Mortensen, J.K., and Fanning, M., 2005, Magmatic and hydrothermal chronology of the giant Rio Blanco porphyry copper deposit, central Chile: implications of an integrated U/Pb and $^{40}Ar/^{39}Ar$ database: Economic Geology, v. 100, p. 905-934.

De Silva, S.L., and Francis, P.W., 1991, Volcanoes of the Central Andes: Berlin, Springer-Verlag, 216 p.

Dilsiz, C., Marques, J.M., and Carreira, P.M.M., 2004, The impact of hydrological changes on travertine deposits related to thermal springs in the Pamukkale area (SW Turkey): Environmental Geology, v. 45, p. 808–817.

Epstein, S., and Mayeda, T.K., 1953, Variations of the $^{18}O/^{16}O$ ratio in natural waters: Geochimica et Cosmochimica Acta, v. 4, p. 213-254.

Ferrara, G.C. Ferrara, G., and Gonfiantini, R., 1963, Carbon isotope composition of carbon dioxide and methane from steam jets of Tuscany, *in* Tongiorgi, E. ed., Nuclear Geology on Geothermal Areas: Pisa, Consiglio Nazionale delle Ricerche, Laboratorio di Geologia Nucleare, p. 275-282.

Fouke, B.W., Farmer, J.D., Des Marais, D.J., Pratt, L., Sturchio, N.C., Burns, P.C., and Discipulo, M.K., 2000, Depositional facies and aqueous-solid geochemistry of travertine-depositing hot springs (Angel terrace, Mammoth Hot Springs, Yellowstone National Park, USA): Journal of Sedimentary Research, v. 70, p. 565-585.

Fournier, R.O., 1989, Geochemistry and dynamics of the Yellowstone National Park hydrothermal system: Annual Review of Earth and Planetary Sciences, v. 17, p. 13-53.

Frank, N., Braum, M., Hambach, U., Mangini, A., and Wagner, G., 2000, Warm Period Growth of Travertine during the Last Interglaciation in Southern Germany: Quaternary Research, v. 54, p. 34-48.

Friedman, I., and O'Neil, J.R., 1977, Compilation of stable isotope fractionation factors of geochemical interest: US Geological Survey, Professional Paper 440-KK, 49 p.

Fritz, S.C., Baker, P.A., Lowenstein, T.K., Seltzer, G.O., Rigsby, C.A., Dwyer, G.S., Tapia, P.M., Arnold, K.K, Ku, T.-L., and Luo, S., 2004, Hydrologic variation during the last 170,000 years in the southern hemisphere tropics of South America: Quaternary Research, v. 61, p. 95-104, DOI: 10.1016/J.YQRES.2003.08.007.

Fritz, S.C., Baker, P.A., Seltzer, G.O., Ballantyne, A., Tapia, P., Cheng, H., and Edwards, R.L., 2007, Quaternary glaciation and hydrologic variation in the South American tropics as reconstructed from the Lake Titicaca drilling project: Quaternary Research, v. 68, p. 410–420.

Garreaud, R., Vuille, M., and Clement, A.C., 2003, The climate of the Altiplano: observed current conditions and mechanisms of the past changes: Palaeogeography, Palaeoclimatology, Palaeoecology v. 194, p. 5-22.

Garrels, R.M., and Lerman, A., 1981, Phanerozoic cycles of sedimentary carbon and sulfur: Proceedings National Academy of Sciences (USA), v. 78, p. 4652-4656.

Godfrey, L.V., Jordan, T.E., Lowenstein, T.K., and Alonso, R.L., 2003, Stable isotope constraints on the transport of water to the Andes between 22º and 26ºS during the last glacial cycle: Palaeogeography, Palaeoclimatology, Palaeoecology, v. 194, p. 299-317.

Goldstein, R.H., and Reynolds, T.J., 1994, Systematics of Fluid Inclusions in Diagenetic Minerals: SEPM, Short Course 31, 199 p.

Hallstadius, S, L., 1984, A method for the electrodeposition of actinides: Nuclear Instruments and Methods in Physics Research, v. 223, p. 266-267.

Hoefs, J., 1997, Stable Isotope Geochemistry: Berlin, Springer, 288 p.

Horita, J., Ueada, A., Mizukami, K., and Takatori, I., 1989, Automatic δD and $\delta^{18}O$ analysis of multiwater samples using H_2- and CO_2-water equilibration methods with a common equilibration set-up: International Journal of Radiation Applications and Instrumentation, v. 40, p. 801-805.

Hulston, J.R., and Mccabe, W.J., 1962, Mass spectrometer measurements in the thermal areas of New Zealand. Part 2. Carbon isotopic ratios: Geochimica et Cosmochimica Acta, v. 26, p. 399-410.

Ingebritsen, S.E., Galloway, D.L., Colvard, E.M., Sorey, M.L., and Mariver, R.H., 2001, Time-variation of hydrothermal discharge at selected sites in the western United States: implications for monitoring: Journal of Volcanology and Geothermal Research, v. 111, p. 1-23.

Jones, B., and Renaut, R.W., 1996, Morphology and growth of aragonite in hot-spring travertines at Lake Bogoria, Kenya Rift Valley: Sedimentology, v. 43, p. 323-340.

Kirshenbaum, I., 1951, Physical properties and analysis of heavy water, *in* Urey H.C., and Murphy G.M., eds., National Nuclear Energy Series, v. 4a: McGraw-Hill, p. 205-249.

Klein, A.G., Seltzer, G.O., and Isacks, B.L., 1999, Modern and last local glacial maximum snowlines in the Central Andes of Peru, Bolivia, and northern Chile: Quaternary Science Reviews, v. 18, p. 63-84.

López-Chicano, M., Ceron, J.C., Vallejos, A., and Pulido-Bosch, A., 2001, Geochemistry of thermal springs. Alhama de Granada (southern Spain): Applied Geochemistry, v. 16, p. 1153-1163.

Marquillas, R., Sabino, I., Sial, A.N., Del Papa, C., Ferreira, V.P., and Matheos, S., 2007, Carbon and oxygen isotopes of Maastrichtian-Danian shallow marine carbonates: Yacoraite Formation, northwestern Argentina: Journal of South American Earth Sciences, v. 23, p. 304-320.

Matteini, M., Mazzuoli, R., Omarini, R., Cas, R., and Maas, R., 2002, Geodynamical evolution of Central Andes at 24ºS as inferred by magma composition along the Calama – Olacapato – El Toro transversal volcanic belt: Journal of Volcanology and Geothermal Research, v. 118, p. 205-228.

Messerli, B., Grosjean, M., Bonani, G., Burgi, A., Geyh, M.A., Graf, K., Ramseyer, K., Romero, H., Schotterer, U., Schreier, H., and Vuille, M., 1993, Climate change and natural resource dynamics of the Atacama Altiplano during the last 18,000 years: A Preliminary Synthesis: Mountain Research and Development, v. 13, no. 2, Mountain Geoecology of the Andes: Resource Management and Sustainable Development, p. 117-127.

Moore, J., Adams, M., Allis, R., Lutz, S., and Rauzi, S., 2005, Mineralogical and geochemical consequences of the long-term presence of CO_2 in natural reservoirs: An example of the Springerville-St.Johns field, Arizona and New Mexico, USA: Chemical Geology, v. 217, p. 365-385.

Ohmoto, H., and Rye, R.O., 1979, Isotope of sulfur and carbon, *in* Barnes, H.L. ed., Geochemistry of Hydrothermal deposits: New York, John Wiley & Sons, p. 509 - 567.

O'Neil, J.R., Clayton, R.N., and Mayeda, T.K., 1969, Oxygen isotope fractionation in divalent metal carbonates: Journal of Chemical Physics, v. 51, p. 5547 - 5558.

Placzek, C., Quade, J., and Patchett, P.J., 2006, Geochronology and stratigraphy of the late Pleistocene lake cycles on the southern Bolivian Altiplano: Implications for causes of tropical climate change: Geological Society of America, Bulletin, v. 118, p. 515-532. doi: 10.1130/B25770.1.

Pentecost, A., 2005, Travertine: Berlin, Springer, 446 p.

Petit, J.R., Jouzel, J., Raynaud, D., Barkov, N.I., Barnola, J.-M., Basile, I., Bender, M.L., Chappellaz, J., Davis, M., Delaygue, G., Delmotte, M., Kotlyakov,V.M., Legrand, M., Lipenkov,V.Y., Lorius, C., Pepin, L., Ritz, C., Saltzman, E., and Stievenard, M., 1999, Climate and atmospheric history of the past 420,000 years from the Vostok ice core, Antarctica: Nature, v. 399, p. 429-437.

Petrinovic, I.A., Riller, U., Brod, J.A., Alvarado, G., and Arnosio, M., 2006, Bimodal volcanism in a tectonic transfer zone: Evidence for tectonically controlled magmatism in the southern Central Andes, NW Argentina: Journal of Volcanology and Geothermal Research, v. 152, p. 240-252. doi: 10.1016/j.jvolgeores.2005.10.008.

Pin, C., and Bassin, C., 1992, Evaluation of a strontium-specific extraction chromatographic method for isotopic analysis in geological materials: Analytica Chimica Acta, v. 269, p. 249-255.

Prokoph, A., Shields, G.A., and Veizer, J., 2008, Compilation and time series analysis of a marine carbonate $\delta^{18}O$, $\delta\ ^{13}C$, $^{87}Sr/^{86}Sr$ and $\delta\ ^{34}S$ database through Earth history: Earth-Science Reviews, v. 87, p. 113-133.

Quade, J., Cerling, T.E., and Bowman, J.R., 1989, Systematic variations in the carbon and oxygen isotopic composition of pedogenic carbonate along elevation transects in the southern Great Basin, United States: Geological Society of America Bulletin, v. 101, p. 464-475.

Renaut, R.E., and Jones, B., 2000, Microbial precipitates around continental hot springs and geysers, *in* Riding R.E., and Awramik S.M., eds., Microbial Sediments: Berlin, Springer, p. 187-195.

Rech, J.A., Quade, J., and Betancourt, J.L., 2002, Late Quaternary paleohydrology of the Central Atacama Desert (lat 22º - 24ºS, Chile): Geological Society of America, Bulletin, v. 114, p. 334-348.

Romanek, C.S., Grossman, E.L., and Morse, J.W., 1992, Carbon isotopic fractionation in synthetic aragonite and calcite: Effects of temperature and precipitation rate: Geochimica et Cosmochimica Acta, v. 56, p. 419-430.

Rondeau, B., 1990, Géochimie isotopique et geochronologie des stromatolites lacustres quaternaries de l'Altiplano bolivien: unpublished doctoral dissertation, Université du Québec, Montreal, 123 p.

Rosenbauer, R.J., 1991, A computer program for the calculation of uranium-series isotopic ages: Computers & Geosciences, v. 17, p. 45-75.

Sáez, A., Valero-Garcés, B.L., Moreno, A., Bao, R., Pueyo, J.J., González-Sampériz, P., Giralt, S., Taberner, C., Herrera, C., and Gibert, R.O., 2007, Lacustrine sedimentation in active volcanic settings: the Late Quaternary depositional evolution of Lake Chungará (northern Chile): Sedimentology, v. 54, p. 1191-1222. doi: 10.1111/j.1365-3091.2007.00878.x.

Sainato, C.M., and Pomposiello, M.C., 1997, Two-dimensional magnetotelluric and gravity models of the Tuzgle volcano zone (Jujuy Province, Argentina): Journal of South American Earth Sciences, v. 10, p. 247-261.

Schwab, K., and Lippolt, H., 1974, K-Ar mineral ages and Late Cenozoic history of Salar de Cauchari area (Argentine Puna), *in* González Ferrán O., ed. Proceedings of the Symposium on Andean and Antarctic Volcanology Problems, Santiago. International Association of Volcanology and Chemistry of the Earth's Interior, Rome, p. 697-714.

Shen, C.C., Edwards, R.L., Cheng, H., Dorale, J.A., Thomas, R.B., Moran, S.B., and Edmonds, H.N., 2002, Uranium and thorium isotopic and concentration measurements by magnetic sector inductively coupled plasma mass spectrometry: Chemical Geology, v. 185, p. 165-178.

Strecker, M.R., Alonso, R.N., Bookhagen, B., Carrapa, B., Hilley, G.E., Sobel, E.R., and Trauth, M.H., 2007, Tectonics and climate of the southern central Andes: Annual Review of Earth and Planetary Sciences, v. 35, p. 747-787. doi: 10.1146/annurev.earth.35.031306.140158.

Talvitie, N.A., 1972, Electrodeposition of actinides for alpha spectrometric determination: Analytical Chemistry, v. 44, p. 280-283.

Taylor, B.E., 1987, Stable isotope geochemistry of ore-forming fluids, *in* Kyser, T.K. ed., Stable Isotope Geochemistry of Low Temperature Fluids: Mineral. Assoc. Can., Short Course, v.13, Mineralogical Society of Canada, Washington, DC, p. 337–445.

Valero-Garcés B.L., Delgado-Huertas A., Ratto, N., and Navas, A., 1999, Large ^{13}C enrichment in primary carbonates from Andean Altiplano lakes, northwest Argentina: Earth and Planetary Science Letters v. 171, p. 253–266.

Valero-Garcés B.L., Arenas C., and Delgado-Huertas A., 2001, Depositional environments of Quaternary lacustrine travertines and stromatolites from high-altitude Andean lakes, northwestern Argentina: Canadian Journal of Earth Sciences, v. 8, p. 1263-1283.

Vengosh, A., Helvaci, C., and Karamandesi, I.H., 2002, Geochemical constraints for the origin of thermal waters from western Turkey: Applied Geochemistry, v. 17, p. 163–183.

Vengosh, A., Helvaci, C., and Karamandesi, I.H., 2003, Reply to the comment on 'Geochemical constraints for the origin of thermal waters from western Turkey' by Umran Serpen and Tahir Öngür: Applied Geochemistry, v. 18, p. 1117–1119.

White, A.F., Peterson. M.L., Wollenberg, H., and Flexer, S., 1990, Sources and fractionation processes influencing the isotopic distribution of H, O and C in the Long Valley hydrothermal system, California, USA: Applied Geochemistry, v. 5, p. 571–585.

Vogel, J.C., 1993, Variability of carbon isotope fractionation during photosynthesis, *in* Ehleringer, J.R., Hall, A.E., and Farquar, G.D., eds, Stable Isotopes and Plant Carbon: San Diego, Academic Press, p. 29-38.

Zhang, T., Zhang, M., Bai, B., Wang, X., and Li, L., 2008, Origin and accumulation of carbon dioxide in the Huanghua Depression, Bohai Bay Basin, China: Geological Society of America, Bulletin, v. 92, p. 341-356.

Zheng, Y.F., 1999, Oxygen isotope fractionation in carbonate and sulphate minerals: Geochemical Journal, v. 33, p. 109-126.

Figure and table captions

Figure 1. Geological map of the study area in the Central Andes (modified from Matteini et al. 2002). The location of the Antuco travertine and the related hot springs are highlighted (not to scale). Present-day thermal water stream flowing to Cauchari salar is also indicated.

Figure 2. Schematic cross- section of the Antuco travertine deposits cropping out along an old quarry front. The relationships between the carbonate units are shown. Present-day thermal water streams along the valley at the foot of the travertine quarry.

Figure 3. A) View of the Lower Travertine showing bedding (upper part) and vertical, palisade-like, calcite pseudomorphs after aragonite (central and lower part). Box corresponds to detail in Part B. B) Detail of longitudinal sections in aragonite pseudomorphs (white forms). C) Basal pseudohexagonal sections of aragonite pseudomorphs. D) Thick section (150 μm thickness) from an aragonite travertine mound in the Antuco Lower Unit. In black is shown the location of individual microsamples. The isotopic composition (vs. V-PDB), in permil, of each microsample is indicated in the boxes.

Figure 4. Interpretive sketch of the paragenetic sequence recorded in the Antuco Lower Travertine (not to scale). Fluid inclusion Groups 1 and 2 are in aragonite crystals and aragonite relics within secondary calcite crystals replacing aragonite. Group 3 of fluid inclusions is found along growth zones in calcite rimming cements. *Stage 1*: Aragonite crystals (a), decimeters in size, are interpreted as formed in pools very close to the thermal vents. Fluid inclusions in aragonite crystals correspond to Group 1 (Th = 87ºC salinity = 3.4 wt% NaCl). *Stage 2*: (A): Calcite (c) precipitated rimming the thermal conduits (b) crossing the Lower Travertine. Fluid inclusions in calcite correspond to Group 3 (Th = 115ºC; salinity = 0.9 wt% NaCl). (B): Replacement of aragonite crystals by sparry calcite (stage 2B). Secondary inclusions in aragonite relics (Group 2 fluid inclusions) show temperatures and salinities similar to those of Group 3 fluid inclusions (in calcite), suggesting similar parental waters.

Figure 5. A) Cross-plot of $\delta^{13}C$ vs. $\delta^{18}O$ values of carbonates from the travertine deposit. Note the isotopic difference between Lower and Upper Travertines. Values from calcite replacing aragonite follow a positive correlation, interpreted to result from cooling and outgassing of thermal waters. These effects were larger in karst-related calcites. B) Plot of age versus $\delta^{18}O_{V\text{-}SMOW}$, illustrating the trends in evolution of parental water of the Antuco travertine deposit. Empty symbols and capital letters correspond to reference waters of the region (meteoric and thermal). Full symbols correspond to calculated isotopic compositions of parental waters. Water evolution in the thermal system during the Late Pleistocene is delimitated between the dashed lines. Precipitation temperature (from fluid-inclusion homogenization temperatures) is indicated for the aragonite in the lower travertine body (LT) and for the conduit-rim calcite cement; $\delta^{18}O$ parental water range for the gray travertines (UT) is also indicated.

Figure 6. Attributes of fluid-inclusion groups identified in the Antuco travertine carbonates. A) Histogram of homogenization temperatures of the fluid-inclusion groups from Antuco travertines. Mean values are annotated. B) Histogram of ice melting temperatures from the Antuco travertine fluid inclusion groups. Mean values (temperature/salinity) are indicated. C) Plot of mean homogenization temperature vs. mean salinity showing the evolution trend of the Antuco thermal waters during precipitation of the Lower Travertine (increase in temperature and decrease in salinity).

Figure 7. Photomicrographs of fluid-inclusion populations under plane-polarized light in a double-polished thick section. A) Example from a large aragonite crystal from travertine mound, illustrating an assemblage of primary two-phase fluid inclusions (Group 1) distributed along the crystallographic *c* axis of aragonite. Group 1 fluid inclusions are intersected by Group 2 fluid inclusions. B) Magnified view of the central box in Part A. C) Magnified view of the central box in Part B. Two-phase primary fluid inclusions of Group 1 are identified by arrows. D) The same view as in Part C but at a different focal plane. Two-phase fluid inclusions are identified by arrows.

Figure 8. Photomicrographs of fluid-inclusion populations under plane-polarized light in a double-polished thick section. A) Assemblage of secondary two-phase fluid inclusions (group 2) in aragonite. B) Magnified view of the central box in Part A. C) Magnified view of the central box in Part B. Location of two-phase fluid inclusions are highlighted by arrows. D) Same view as in Part C at a different focal plane. Two-phase fluid inclusions following cleavage planes are marked by arrows.

Figure 9. Photomicrographs of fluid-inclusion populations under plane-polarized light in a double-polished thick section. A) Growth zones in a calcite crystal within a thermal conduit. Arrows indicate the growth direction. B) Magnified view of central box in Part A. Two-phase primary fluid inclusions are arranged following the crystal growth zonation. (C, D) Magnified view of the respective boxes in Part B. Two-phase fluid inclusions are highlighted by arrows.

Figure 10. Plot of $^{87}Sr/^{86}Sr$ vs. $\delta^{13}C$ from the Antuco travertines (lower and upper bodies). Compositions of marine carbonates (lower Ordovician, lower Permian, and upper Cretaceous in age) are marked as rectangles for reference. Also indicated are the ranges of: (1) common $\delta^{13}C$ values for deep-seated magmatic CO_2 (White et al. 1990; Zhang et al. 2008), and (2) common $^{87}Sr/^{86}Sr$ values corresponding to thermal recycling of old marine carbonates (Vengosh et al. 2002). The values of the Antuco travertines suggest a magmatic provenance.

Figure 11. Sketch of the accretionary stages recorded in the Antuco travertines and their links to climatic records. A) Main growth phases in the Antuco travertine, illustrating the relative water availability for each growth phase. B) Marine isotope stages (MIS) and the Vostok CO_2 record (Petit et al. 1999). C) High and low lake level periods in the Altiplano lakes, reflecting humid and arid periods, are represented. Uyuni Lake changes are based mostly on the percent carbonate content (Fritz et al. 2004, Placzek et al. 2006). Atacama Lake changes are based in the lithofacies distribution (Bobst et al. 2001). Lake Titicaca changes are based on % of freshwater diatom

variations (Fritz et al. 2007). Dashed bars in Part B correspond to $^{238}U/^{230}Th$ date uncertainties (see Tables 1 and 2).

Table 1. Uranium and thorium isotopic compositions and ^{230}Th ages for the Lower Antuco Travertines (LT).

Table 2. Uranium and thorium isotopic compositions and ^{230}Th ages for the Upper Antuco Travertines (UT).

Table 3. Fluid-inclusion data set of FI groups identified in the Antuco travertine carbonates.

Data archive. Carbon and oxygen isotopic composition of micromilled samples from the Antuco travertine deposit. The last two columns of the table indicate precipitation temperature (measured from fluid inclusions) and $\delta^{18}O_{V\text{-}SMOW}$ values of parental water in equilibrium with carbonate precipitates (aragonite and calcite) at the measured temperatures.

[1] Precipitation temperatures measured *in situ* and calculated $\delta^{18}O_{V\text{-}SMOW}$ values of parental water in equilibrium with carbonate (aragonite and calcite) at this temperature.

[2] Calculated precipitation temperatures of grey travertines (see text for details) according to the $\delta^{18}O_{V\text{-}SMOW}$ parental water range. First row (in italics), minimum precipitation temperature, and second row (in bold), maximum precipitation temperature.

[3] Homogenization temperatures of primary two-phase fluid inclusions (Group 3).

[4] Homogenization temperatures of primary two-phase fluid inclusions (Group 1).

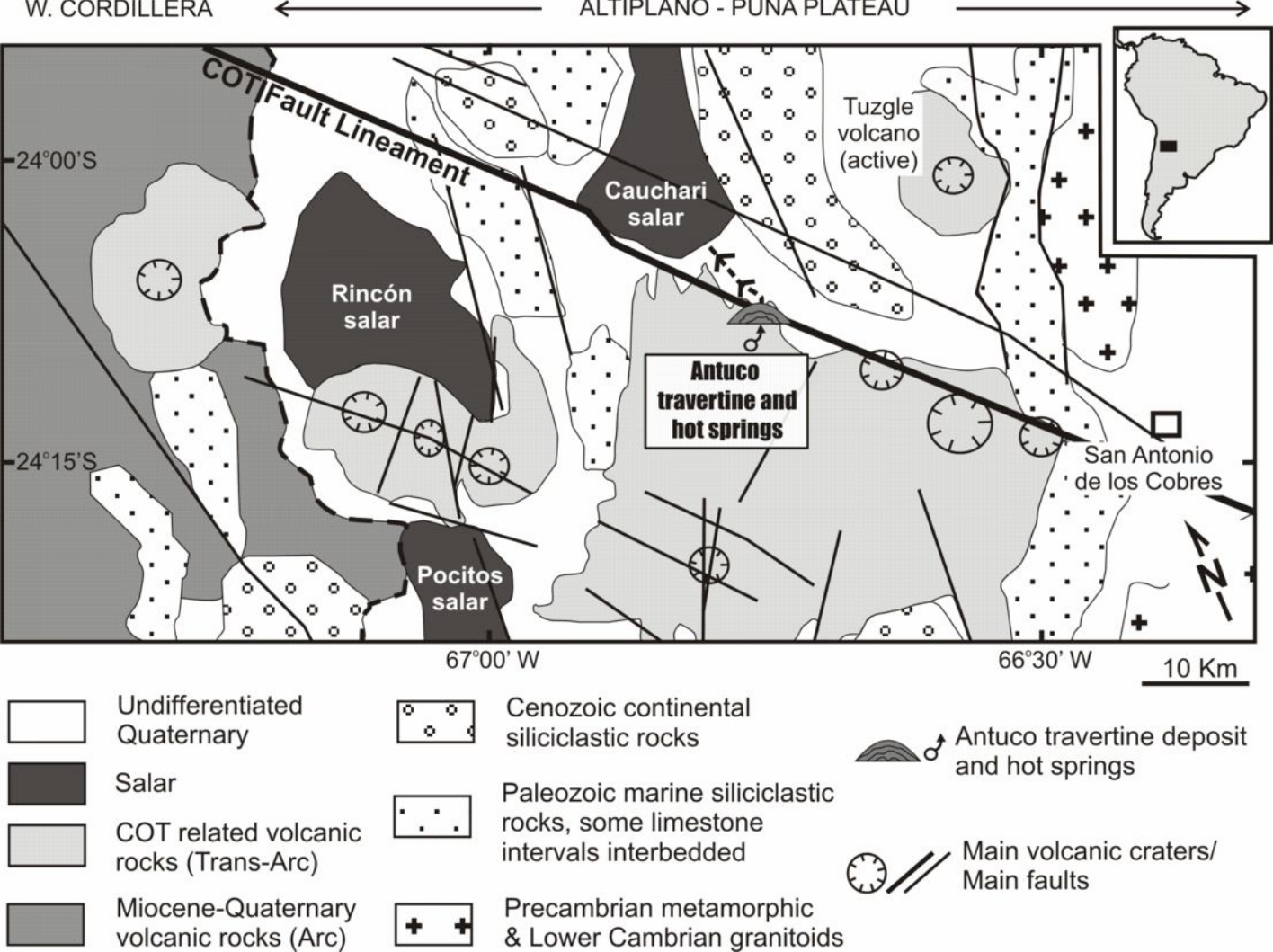
W. CORDILLERA
ALTIPLANO - PUNA PLATEAU
COT Fault Lineament
Tuzgle volcano (active)
Cauchari salar
Rincón salar
Antuco travertine and hot springs
San Antonio de los Cobres
Pocitos salar
24°00'S
24°15'S
67°00' W
66°30' W
10 Km
Undifferentiated Quaternary
Salar
COT related volcanic rocks (Trans-Arc)
Miocene-Quaternary volcanic rocks (Arc)
Cenozoic continental siliciclastic rocks
Paleozoic marine siliciclastic rocks, some limestone intervals interbedded
Precambrian metamorphic & Lower Cambrian granitoids
Antuco travertine deposit and hot springs
Main volcanic craters/ Main faults


A

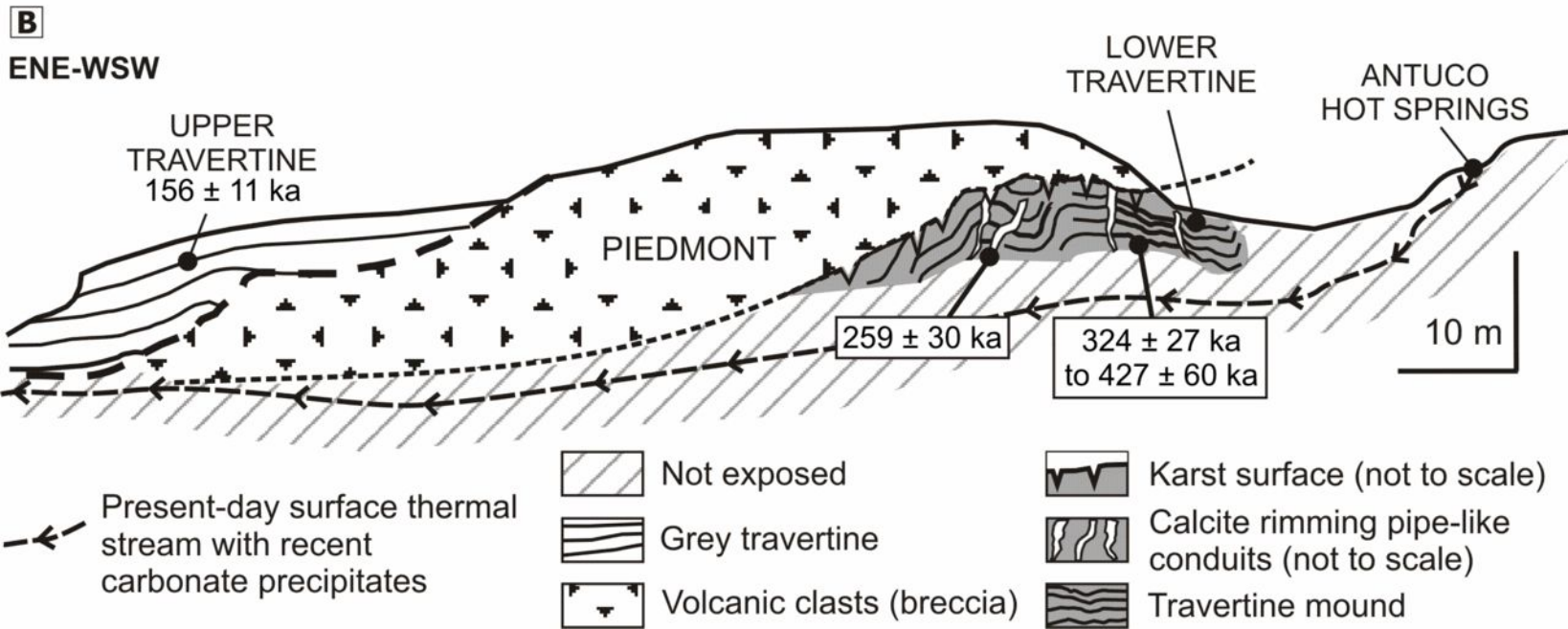
B
ENE-WSW
UPPER TRAVERTINE 156 ± 11 ka
PIEDMONT
LOWER TRAVERTINE
ANTUCO HOT SPRINGS
259 ± 30 ka
324 ± 27 ka to 427 ± 60 ka
10 m
Present-day surface thermal stream with recent carbonate precipitates
Not exposed
Grey travertine
Volcanic clasts (breccia)
Karst surface (not to scale)
Calcite rimming pipe-like conduits (not to scale)
Travertine mound

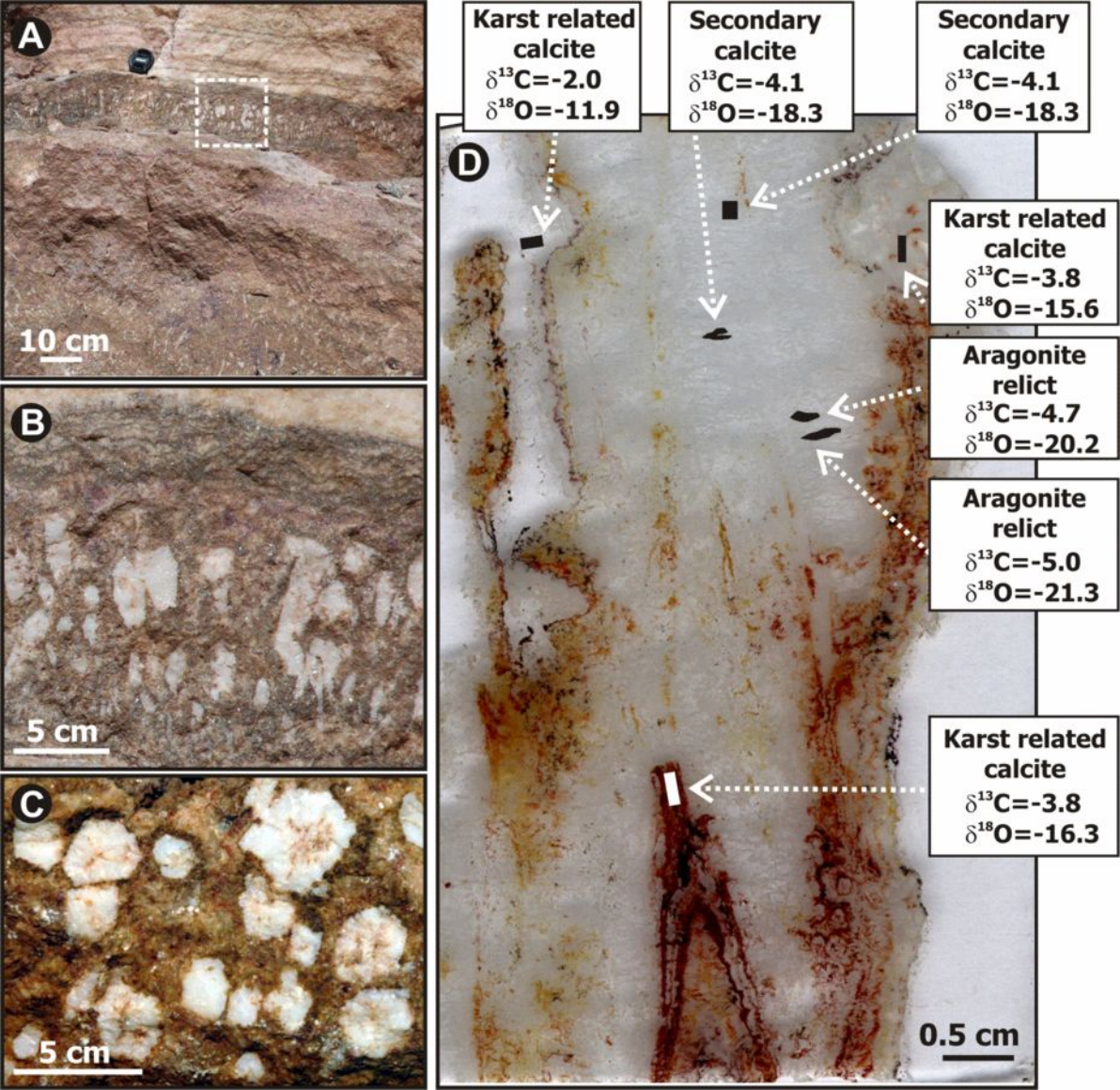
A
10 cm
B
5 cm
C
5 cm
D
Karst related calcite
δ13C=-2.0
δ18O=-11.9
Secondary calcite
δ13C=-4.1
δ18O=-18.3
Secondary calcite
δ13C=-4.1
δ18O=-18.3
Karst related calcite
δ13C=-3.8
δ18O=-15.6
Aragonite relict
δ13C=-4.7
δ18O=-20.2
Aragonite relict
δ13C=-5.0
δ18O=-21.3
Karst related calcite
δ13C=-3.8
δ18O=-16.3
0.5 cm

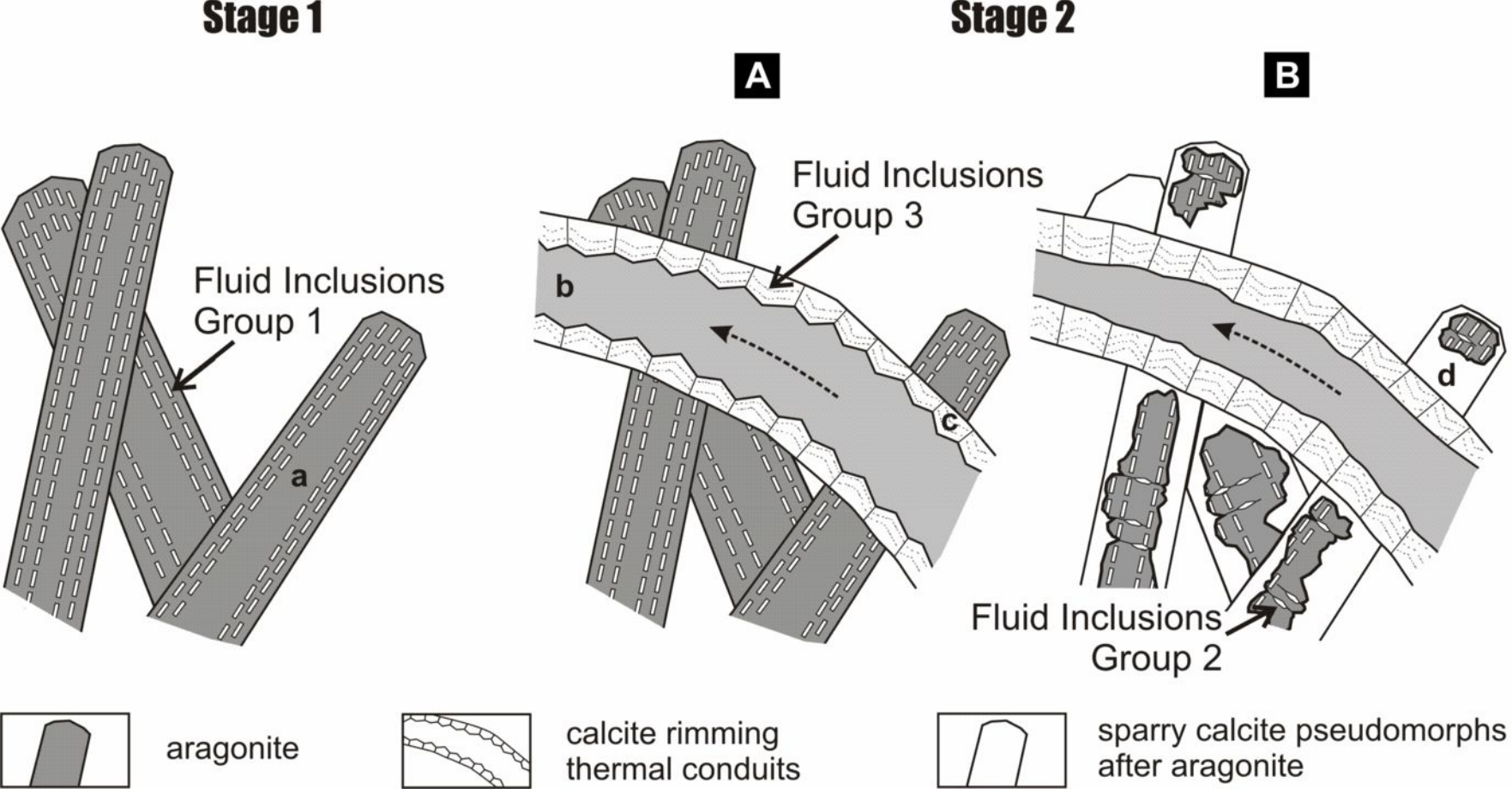
Stage 1
Stage 2
A
B
Fluid Inclusions
Group 1
a
b
Fluid Inclusions
Group 3
c
d
Fluid Inclusions
Group 2
aragonite
calcite rimming
thermal conduits
sparry calcite pseudomorphs
after aragonite

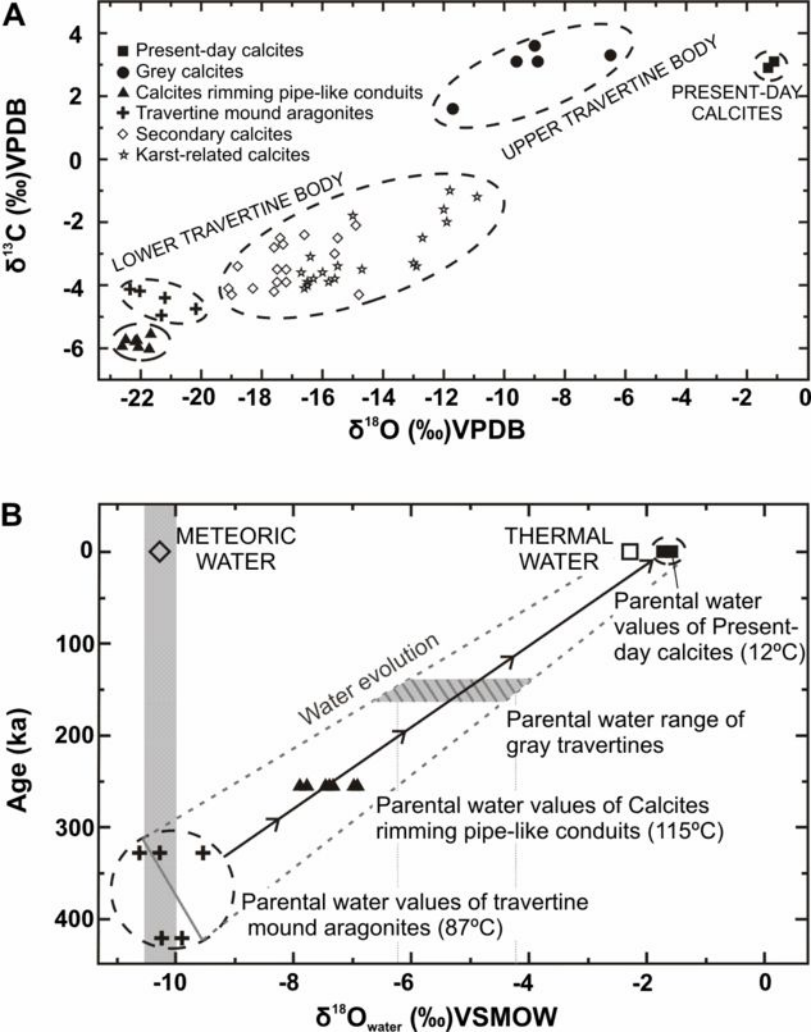
A
Present-day calcites
Grey calcites
Calcites rimming pipe-like conduits
Travertine mound aragonites
Secondary calcites
Karst-related calcites
UPPER TRAVERTINE BODY
PRESENT-DAY CALCITES
LOWER TRAVERTINE BODY
δ13C (‰)VPDB
δ18O (‰)VPDB
B
METEORIC WATER
THERMAL WATER
Parental water values of Present-day calcites (12ºC)
Water evolution
Parental water range of gray travertines
Parental water values of Calcites rimming pipe-like conduits (115ºC)
Parental water values of travertine mound aragonites (87ºC)
Age (ka)
δ18Owater (‰)VSMOW

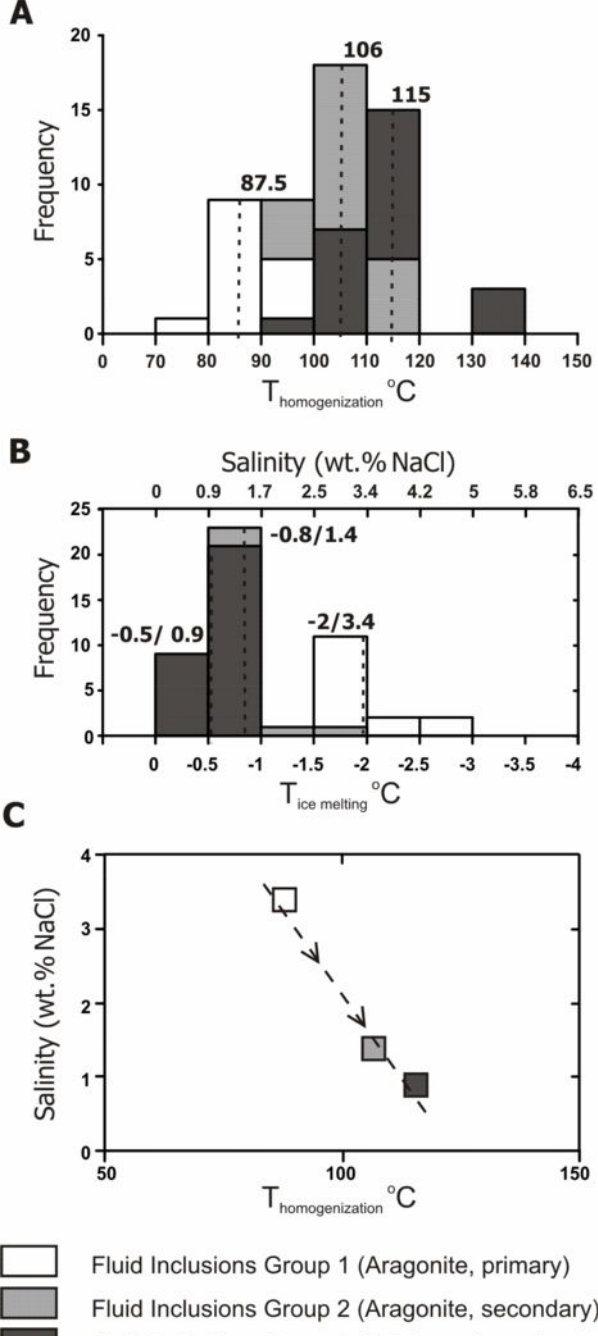
A
Frequency
106
115
87.5
T homogenization °C
B
Salinity (wt.% NaCl)
Frequency
-0.8/1.4
-0.5/ 0.9
-2/3.4
T ice melting °C
C
Salinity (wt.% NaCl)
T homogenization °C
Fluid Inclusions Group 1 (Aragonite, primary)
Fluid Inclusions Group 2 (Aragonite, secondary)
Fluid Inclusions Group 3 (Calcite, primary)

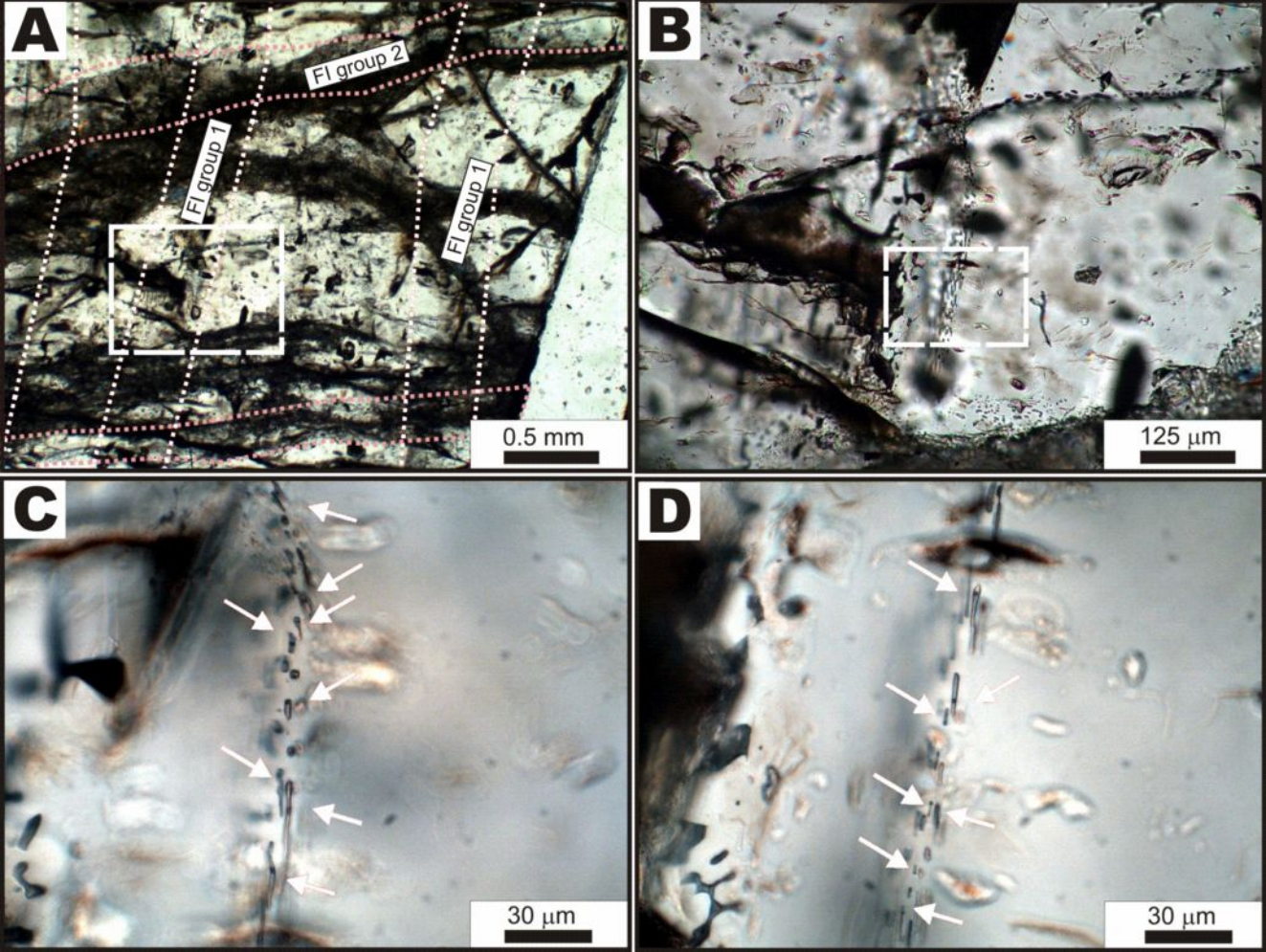
A
FI group 2
FI group 1
FI group 1
0.5 mm
B
125 μm
C
30 μm
D
30 μm

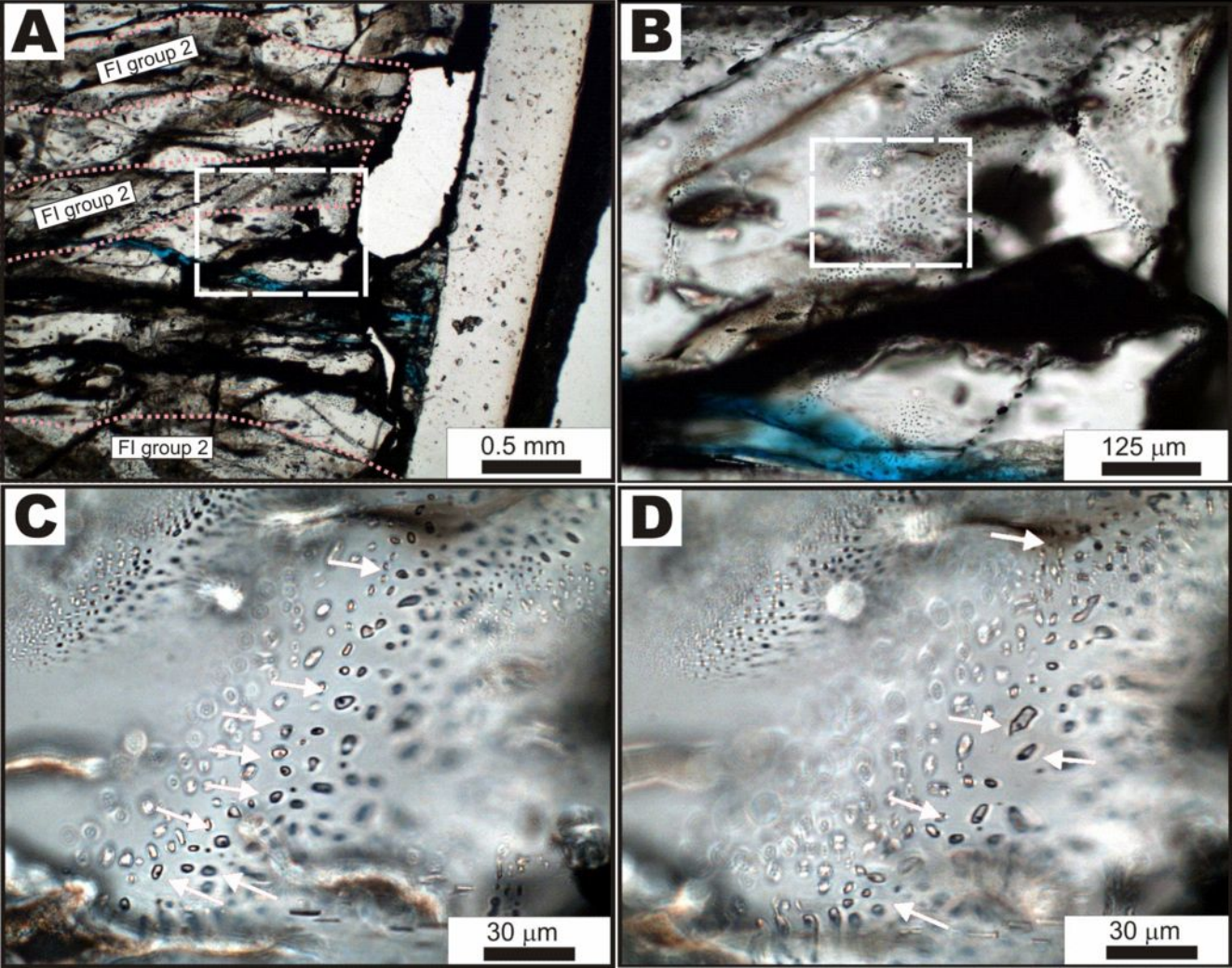
A
FI group 2
FI group 2
FI group 2
0.5 mm
B
125 μm
C
30 μm
D
30 μm

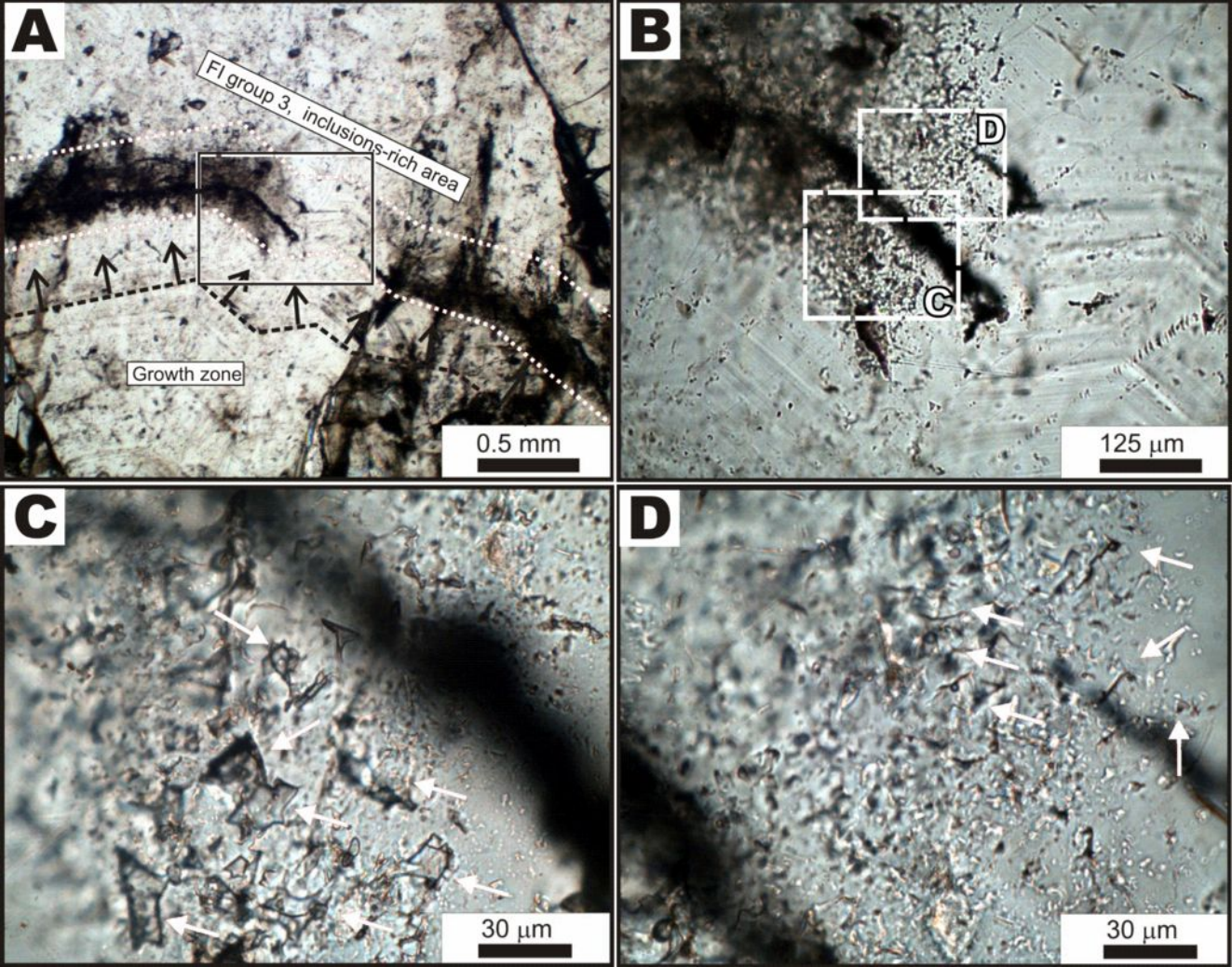
A
FI group 3, inclusions-rich area
Growth zone
0.5 mm
B
D
C
125 µm
C
30 µm
D
30 µm

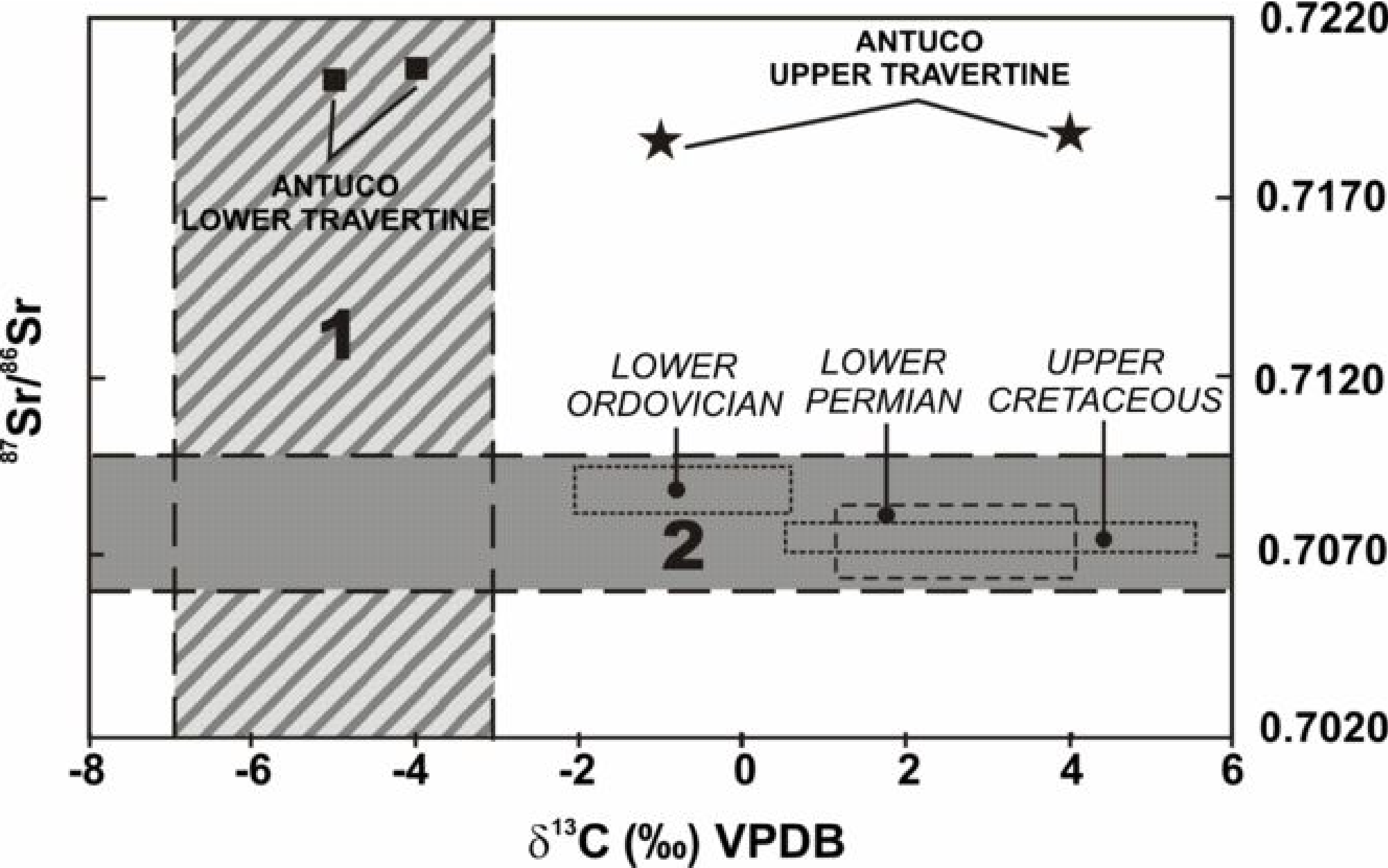
ANTUCO
UPPER TRAVERTINE
ANTUCO
LOWER TRAVERTINE
1
2
LOWER
ORDOVICIAN
LOWER
PERMIAN
UPPER
CRETACEOUS
0.7220
0.7170
0.7120
0.7070
0.7020
-8
-6
-4
-2
0
2
4
6
$^{87}Sr/^{86}Sr$
$\delta^{13}C$ (‰) VPDB

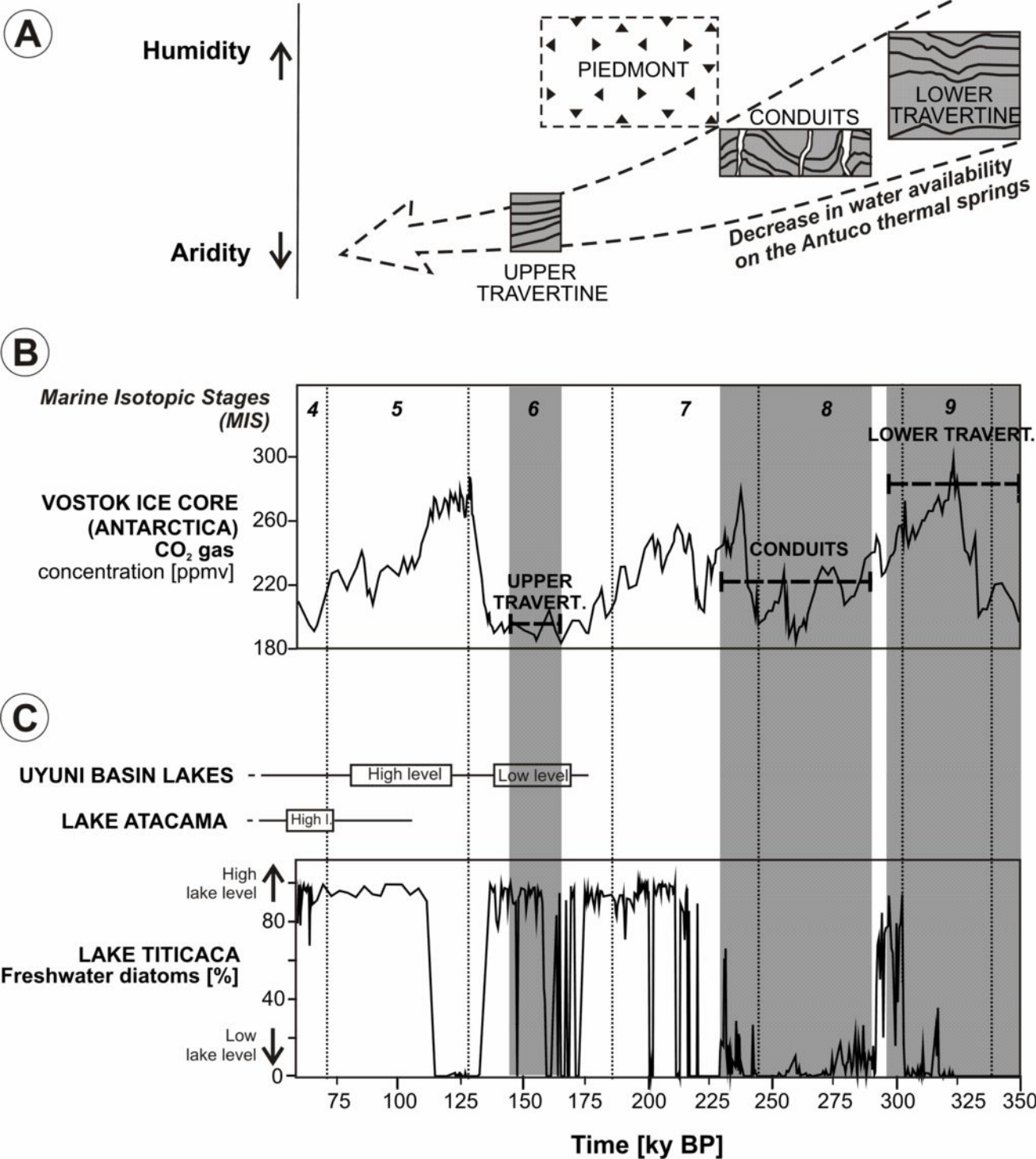
A
Humidity
Aridity
PIEDMONT
CONDUITS
LOWER TRAVERTINE
UPPER TRAVERTINE
Decrease in water availability on the Antuco thermal springs
B
Marine Isotopic Stages (MIS)
4
5
6
7
8
9
LOWER TRAVERT.
300
260
220
180
VOSTOK ICE CORE (ANTARCTICA)
CO2 gas
concentration [ppmv]
UPPER TRAVERT.
CONDUITS
C
UYUNI BASIN LAKES
High level
Low level
LAKE ATACAMA
High l.
High lake level
80
40
Low lake level
0
LAKE TITICACA
Freshwater diatoms [%]
75
100
125
150
175
200
225
250
275
300
325
350
Time [ky BP]

Table 1

Facies	^{238}U ppb	^{232}Th ppt	$\delta^{234}U$ measured[1]	$[^{230}Th/^{238}U]$ activity[2]	$[^{230}Th/^{232}Th]$ ppm	Age corrected (ky BP)[3]	$\delta^{234}U$ initial[4]
Calcite rimming pipe-like conduit	7.3 ± 0.1	34 ± 9	47±16	0.9610 ± 0.0212	3394	259 ± 30	96.7 ± 34
Travertine mound aragonite	28.2 ± 0.1	51 ± 11	63±9	1.0283 ± 0.0090	9299	324 ± 26.5	158 ± 25.5
Travertine mound aragonite	53.1 ± 0.2	233 ± 16	57±8	1.0525 ± 0.0166	3966	409 ± 85	181 ± 70
Travertine mound aragonite	31.2 ± 0.1	75 ± 9	30±6	1.0217 ± 0.0085	7004	426.5 ± 60.5	103 ± 31

Analytical errors are 2s of the mean.

[1] $\delta^{234}U = ([^{234}U/^{238}U]_{activity} - 1) \times 1000$.

[2] $[^{230}Th/^{238}U]_{activity} = 1 - e^{-\lambda_{230}T} + (\delta^{234}U_{measured}/1000)[\lambda_{230}/(\lambda_{230} - \lambda_{234})](1 - e^{-(\lambda_{230} - \lambda_{234})T})^3$, where *T* is the age.
Decay constants are 9.1577×10^{-6} yr^{-1} for ^{230}Th, 2.8263×10^{-6} yr^{-1} for ^{234}U [4], and 1.55125×10^{-10} yr^{-1} for ^{238}U [5].

[3] Age corrections were calculated using an average crustal $^{230}Th/^{232}Th$ atomic ratio of $4.4 \times 10^{-6} \pm 2.2 \times 10^{-6}$. Those are the values for a material at secular equilibrium, with the crustal $^{232}Th/^{238}U$ value of 3.8 and the errors were arbitrarily assumed to be 50%.

[4] $\delta^{234}U_{initial}$ corrected was calculated based on ^{230}Th age (T), i.e., $\delta^{234}U_{initial} = \delta^{234}U_{measured} Xe^{\lambda 234 * T}$, where T is corrected age.

Table 2

Facies	^{238}U ppm	^{232}Th ppm	$[^{234}U/^{238}U]$ activity	$[^{230}Th/^{234}U]$ activity	$[^{230}Th/^{232}Th]$ ppm	Age corrected (ky BP)
Gray calcite	2.16	0.23	1.52 ± 0.02	0.81 ± 0.03	35.66 ± 1.3	156 ± 11
Gray calcite	2.32	0.73	1.51 ± 0.01	0.80 ± 0.02	11.92 ± 0.24	152 ± 9

Table 3

Sample	n	V/L Ratio (%)		FI size (μm)		Homog. T(ºC)		Salinity (wt.% NaCl)	
		mean	range	mean	range	mean	range	mean	range
Aragonite									
FIGr 1	15	9.3	11 to 9	15.5	20 to 12	87.5	98 to 75.6	3.4	4.5 to 3.1
FIGr 2	33	8.1	12 to 6	7.9	20 to 5	106.5	110 to 95.2	1.4	2.6 to 1.1
Calcite									
FIGr 3	28	7.0	12 to 5	8.9	15 to 4	115.2	132 to 103	0.9	1.1 to 0.5

Data archive

Travertine Facies	$\delta^{13}C$ ‰ VPDB	$\delta^{18}O$ ‰ VPDB	T (ºC)	$\delta^{18}O$ ‰ VSMOW
Present day calcite	2.9	-1.3	12[1]	-1.7
Present day calcite	3.1	-1.1	12[1]	-1.5
Gray tufaceous calcite	3.3	-6.5	*16*[2]	*-6.1*
Gray tufaceous calcite	3.3	-6.5	**25**[2]	**-4.2**
Gray tufaceous calcite	3.6	-9	*28*[2]	*-6.1*
Gray tufaceous calcite	3.6	-9	**38**[2]	**-4.2**
Gray tufaceous calcite	3.1	-8.9	*27*[2]	*-6.2*
Gray tufaceous calcite	3.1	-8.9	**37**[2]	**-4.2**
Gray tufaceous calcite	1.6	-11.7	*43*[2]	*-6.1*
Gray tufaceous calcite	1.6	-11.7	**54**[2]	**-4.2**
Gray tufaceous calcite	3.1	-9.6	*31*[2]	*-6.1*
Gray tufaceous calcite	3.1	-9.6	**41**[2]	**-4.2**
Calcite rimming pipe-like conduit	-5.5	-21.7	115[3]	-6.9
Calcite rimming pipe-like conduit	-5.7	-22.5	115[3]	-7.8
Calcite rimming pipe-like conduit	-6.0	-21.7	115[3]	-7.0
Calcite rimming pipe-like conduit	-5.7	-22.1	115[3]	-7.4
Calcite rimming pipe-like conduit	-5.7	-22.2	115[3]	-7,5
Calcite rimming pipe-like conduit	-5.9	-22.1	115[3]	-7.4
Calcite rimming pipe-like conduit	-5.9	-22.6	115[3]	-7.9
Travertine mound aragonite	-4.2	-22.0	88[4]	-10.4
Travertine mound aragonite	-5.0	-21.3	88[4]	-9.7
Travertine mound aragonite	-4.1	-22.4	88[4]	-10.8
Travertine mound aragonite	-4.7	-20.2	88[4]	-8.5
Travertine mound aragonite	-4.4	-21.2	88[4]	-9.4
Karst related calcite	-3.3	-13		
Karst related calcite	-2	-11.9		
Karst related calcite	-3.6	-16		
Karst related calcite	-4.1	-16.6		
Karst related calcite	-1	-11.8		
Karst related calcite	-1.2	-10.9		
Karst related calcite	-1.8	-15		
Karst related calcite	-3.4	-12.9		
Karst related calcite	-3.3	-13		
Karst related calcite	-3.6	-16.7		
Karst related calcite	-2.5	-12.7		
Karst related calcite	-3.8	-15.6		
Karst related calcite	-3.9	-15.8		
Karst related calcite	-3.4	-15.5		
Karst related calcite	-3.8	-16.3		
Karst related calcite	-3.8	-16.3		
Karst related calcite	-4.0	-16.5		
Karst related calcite	-3.9	-16.5		
Karst related calcite	-3.1	-16.4		
Karst related calcite	-1.6	-12.0		
Karst related calcite	-3.5	-14.7		
Secondary calcite (Pseudom. aragonite)	-3.9	-17.5		
Secondary calcite (Pseudom. aragonite)	-3.0	-15.6		
Secondary calcite (Pseudom. aragonite)	-3.9	-17.2		
Secondary calcite	-4.3	-14.8		
Secondary calcite (Pseudom. aragonite)	-3.5	-17.2		
Secondary calcite (Pseudom. aragonite)	-4.1	-18.3		
Secondary calcite (Pseudom. aragonite)	-4.2	-17.6		
Secondary calcite (Pseudom. aragonite)	-3.5	-17.5		
Secondary calcite	-2.7	-17.3		
Secondary calcite	-2.5	-17.4		
Secondary calcite	-2.5	-15.5		
Secondary calcite	-2.4	-16.6		
Secondary calcite	-2.8	-17.6		
Secondary calcite	-2.1	-14.9		
Secondary calcite (Pseudom. aragonite)	-4.3	-19		
Secondary calcite (Pseudom. aragonite)	-3.4	-18.8		
Secondary calcite (Pseudom. aragonite)	-4.1	-19.1		